Cell Transplantation
2018, Vol. 27(6) 916–936

DOI: 10.1177/0963689718759463
journals.sagepub.com/home/cll
SAGE

Bone Marrow CD133$^+$ Stem Cells Ameliorate Visual Dysfunction in Streptozotocin-induced Diabetic Mice with Early Diabetic Retinopathy

Liyuan Rong[1,2], Xianliang Gu[1,2], Jing Xie[1,2], Yuxiao Zeng[1,2], Qiyou Li[1,2], Siyu Chen[1,2], Ting Zou[1,2], Langyue Xue[1,2], Haiwei Xu[1,2], and Zheng Qin Yin[1,2]

Abstract

Diabetic retinopathy (DR), one of the leading causes of vision loss worldwide, is characterized by neurovascular disorders. Emerging evidence has demonstrated retinal neurodegeneration in the early pathogenesis of DR, and no treatment has been developed to prevent the early neurodegenerative changes that precede detectable microvascular disorders. Bone marrow CD133$^+$ stem cells with revascularization properties exhibit neuroregenerative potential. However, whether CD133$^+$ cells can ameliorate the neurodegeneration at the early stage of DR remains unclear. In this study, mouse bone marrow CD133$^+$ stem cells were immunomagnetically isolated and analyzed for the phenotypic characteristics, capacity for neural differentiation, and gene expression of neurotrophic factors. After being labeled with enhanced green fluorescent protein, CD133$^+$ cells were intravitreally transplanted into streptozotocin (STZ)-induced diabetic mice to assess the outcomes of visual function and retina structure and the mechanism underlying the therapeutic effect. We found that CD133$^+$ cells co-expressed typical hematopoietic/endothelial stem/progenitor phenotypes, could differentiate to neural lineage cells, and expressed genes of robust neurotrophic factors in vitro. Functional analysis demonstrated that the transplantation of CD133$^+$ cells prevented visual dysfunction for 56 days. Histological analysis confirmed such a functional improvement and showed that transplanted CD133$^+$ cells survived, migrated into the inner retina (IR) over time and preserved IR degeneration, including retina ganglion cells (RGCs) and rod-on bipolar cells. In addition, a subset of transplanted CD133$^+$ cells in the ganglion cell layer differentiated to express RGC markers in STZ-induced diabetic retina. Moreover, transplanted CD133$^+$ cells expressed brain-derived neurotrophic factors (BDNFs) in vivo and increased the BDNF level in STZ-induced diabetic retina to support the survival of retinal cells. Based on these findings, we suggest that transplantation of bone marrow CD133$^+$ stem cells represents a novel approach to ameliorate visual dysfunction and the underlying IR neurodegeneration at the early stage of DR.

Keywords

Diabetic retinopathy, CD133$^+$ cells, visual function, retina degeneration, cell transplantation

Introduction

Diabetic retinopathy (DR), the most common vision-threatening complication of diabetes mellitus (DM), is one of the leading causes of blindness among working-aged adults worldwide[1–3]. The prevalence of DR continues to increase due to the increasing DM population, which is estimated to increase to 552 million worldwide by 2030[4]. Patients with DR suffer severe sight-threatening stages, including diabetic macular edema (DME) and proliferative diabetic retinopathy[1]. DR also confers a high risk of life-threatening vascular damage, such as stroke and heart disease, to DM patients[2].

DR is primarily characterized by gradually progressive retinal vascular disorders involving dysfunction and loss of

[1] Southwest Hospital, Southwest Eye Hospital, Third Military Medical University (Army Medical University), Chongqing, China
[2] Key Lab of Visual Damage and Regeneration & Restoration of Chongqing, Chongqing, China

Submitted: December 14, 2017. Revised: January 15, 2018. Accepted: January 22, 2018.

Corresponding Authors:
Haiwei Xu, Southwest Hospital, Southwest Eye Hospital, Third Military Medical University (Army Medical University), 30 Gaotanyan ST, Shapingba District, Chongqing, 400038, China.
Email: haiweixu2001@163.com
Zheng Qin Yin, Southwest Hospital, Southwest Eye Hospital, Third Military Medical University (Army Medical University), 30 Gaotanyan ST, Shapingba District, Chongqing, 400038, China.
Email: qinzyin@aliyun.com

endothelial cells and pericytes, which causes damage to retinal vascular integrity[5], resulting in blood–retinal barrier breakdown, hemorrhage, neovascularization and ultimately blindness[5,6]. Nevertheless, mounting evidence has demonstrated that retina neurodegeneration occurs earlier before the onset of any visible vascular changes[7–10], and may participate in the development of microvascular damage[8]. Thus, DR was recently proposed as a neurovascular degenerative disease involving the retina[9,11,12].

Although the underlying mechanisms by which DM induces neuronal degeneration and dysfunction in retina are still not clear, the survival and function of retinal neurons seem to be independently affected by hyperglycemia[8]. Emerging evidence has demonstrated that neuronal death in the inner retina (IR), which contributes largely to the impaired visual functions[7] and reduced retina thickness[13,14] in the development of DR, can be detected before microvascular abnormalities[7]. Retina ganglion cells (RGCs) and rod-on bipolar cells (RBCs), located in the IR, have been reported to be the most vulnerable cells in diabetes[8,15]. Loss of these cells results in impaired retinal electrophysiological responses, visual acuity and contrast sensitivity[8,15,16]. In addition, many studies have demonstrated that the downregulation of neuroprotective factors compromises the neuroprotection against diabetic-induced neuronal damages in the diabetic retina, including nerve growth factor (NGF), brain-derived neurotrophic factor (BDNF), glial-derived neurotrophic factor (GDNF), and ciliary neurotrophic factor (CNTF), thereby accelerating neuronal death[8].

Current treatments for DR including laser photocoagulation, intravitreal anti-vascular endothelial growth factor, corticosteroids and vitreoretinal surgery, however, are focused on the late-stage vascular changes that severely impeding visions, such as DME, hemorrhage, or fibrosis[5,17], and show limited success and cause unavoidable side effects[5,8,18]. In addition, there is no agreed treatment to delay disease progression, particularly at earlier stages, before these approaches are applied[19].

Recent clinical trials for retinal degenerative disease, such as age-related macular degeneration or retinitis pigmentosa, have proven stem cell therapy to be safe and efficient[20,21]. The similarities among these degenerative diseases and DR in terms of neuronal loss[9,22] and lacked endogenous regenerative mechanisms[22–24] have inspired investigations of cell-based therapies for DR[6,25]. Previous stem cell transplantation studies on DR[26–32], such as mesenchymal stem cells (MSCs)[26–28,33] or vascular progenitor cells[29,30], have reported efficacy for vascular restorations. However, the effects of these cells on neural disorders are controversial[26,27,31]. In addition, the type of stem cell that is appropriate for DR treatment remains to be elucidated[25].

CD133 (prominin-1/AC133), a stem cell marker[34,35], has been detected in hematopoietic stem/progenitor cells (HSCs/HPCs), neuroepithelial stem cells[34], epithelial progenitor cells (EPCs)[36], lung progenitor cells[37] and cancer stem cells[34]. CD133-positive ($CD133^+$) cells can self-renew and differentiate into cells of three germ layers[34] and can secret abundant trophic and immunosuppressive factors[37–39]. This regenerative potential of $CD133^+$ cells is appealing for applications in ischemic or neural disease and has demonstrated success[40–42]. Moreover, $CD133^+$ cell isolation from bone marrow or peripheral blood is relatively safe, with limited ethical concerns[25]. Recent studies on neural disorders including spinal injury[39,42] and stroke[38] have proven that, $CD133^+$ cells exhibit prominent neuroregenerative potential, displaying enhanced axonal growth and functional restoration compared with $CD133^-$ cells[39]. However, the therapeutic effect of $CD133^+$ cells against neurodegeneration in DR has not yet been assessed.

These findings prompted us to hypothesize that the intravitreal transplantation of $CD133^+$ stem cells from mouse bone marrow might prevent retina degeneration and visual dysfunctions in streptozotocin (STZ)-induced type 1 diabetic mice with early-stage DR. Furthermore, the therapeutic effect of these cell-based regenerative events was monitored to investigate the underlying mechanisms. Our results demonstrated that $CD133^+$ cells, representing a hematopoietic/endothelial progenitor population in the bone marrow, are capable of expressing neurotrophic factor genes and differentiating into neural-like cells in vitro. Transplanted $CD133^+$ cells survive and migrate into the IR, partially differentiate to express neural markers, increase the BDNF level in the retina, prevent IR degeneration including abnormal RBC and RGC loss and, thus, contribute to visual rehabilitation of impaired electroretinogram (ERG) and optomotor responses in STZ mice with early DR.

Materials and Methods

Animals and Diabetes Induction

All animals were housed according to the Third Military Medical University (TMMU) guidelines. All animal protocols were conducted according to the guidance approved by the Institutional Animal Care and Use Committee of TMMU. C57BL/6 mice were housed at constant temperature and humidity under a 12-h light/dark cycle and fed standard diet and water.

The 8-week-old male C57BL/6 mice were randomly assigned to receive a single intraperitoneal (i.p.) injection of 150 mg/kg STZ (Sigma-Aldrich, St. Louis, MO, USA) or vehicle (0.1 M citrate buffer, pH 4.5) as previously described[14]. The fasting blood glucose (FBG) level was measured with an Accu-Chek Performa glucometer system (Roche Diagnostic, Mannheim, Germany) using blood from the tail vein and the weights were recorded before each experiment after fasting for at least 4 hours. Mice with FBG level >16.7 mmol/l 2 days after STZ injection were regarded as diabetic mice and were included in the experiments. The injection day was regarded as day 0.

Isolation and Expansion of Mouse Bone Marrow-Derived CD133$^+$ Stem Cells

The tibias and femurs from 8-week-old male C57BL/6 mice were extracted, and the bone marrow was flushed as described previously[43]. Bone marrow mononuclear cells (BMNCs) were then isolated by density-gradient centrifugation with Ficoll-Paque PREMIUM 1.084 (GE Healthcare, Little Chalfont, United Kingdom). CD133$^+$ cells were separated from BMNCs with anti-mouse-prominin-1 microbeads (Miltenyi MACS; Miltenyi Biotec, Auburn, CA, USA) using a magnetically activated cell sorter (Miltenyi Biotec). Freshly isolated cells were seeded at 2×10^5 cells/well in 24-well plates (NEST, China) pre-coated with 0.015 mg/ml poly-L-lysine (PLL; Sigma-Aldrich) and vitronectin (Gibco, Invitrogen, Carlsbad, CA, USA). The cells were then cultured in alpha minimal essential medium (αMEM) supplemented with 10% fetal bovine serum (FBS), 100 IU/ml penicillin, 100 mg/ml streptomycin (Gibco), 100 ng/ml stem cell factor, 100 ng/ml FMS-like tyrosine kinase-3 ligand, 20 ng/ml interleukin-6 and 20 ng/ml leukemia inhibitory factor (PeproTech, Rocky Hill, NJ, USA) according to previous studies with slight modifications[39,44–46] at 37°C in a humidified atmosphere containing 5% CO_2. The cells were harvested with 0.05% trypsin/ethylenediaminetetraacetic acid (EDTA; Invitrogen) before passaging.

Phenotypes of CD133$^+$ cells

To analyze the purity and phenotypes of CD133$^+$ cells before and after isolation, flow cytometry was performed as described previously[47]. Briefly, either whole BMNCs, or CD133$^+$ cells from freshly isolated or different passages were incubated with mouse CD133 (phycoerythrin [PE]-conjugated; Miltenyi Biotec/eBioscience), CD34 (fluorescein isothiocyanate-conjugated), CD45, CD117 (c-kit), CD184 (CXCR4), CD31, CD309 (vascular endothelial growth factor receptor (VEGFR)2/kinase insert domain receptor (KDR)), CD90, and major histocompatibility complex (MHC) II (all allophycocyanin [APC]-conjugated) antibodies or matched isotype controls (Miltenyi Biotec). Cells were then analyzed using a FACSCalibur Flow Cytometer (BD Bioscience, San Jose, CA, USA). At least 10,000 cells were collected for each sample and analyzed using FlowJo software (Ashland, OR, USA).

Proliferation Assays of CD133$^+$ Cells

The cells were cultured for analyses of morphology changes and population doubling time among different passages. All phase-contrast pictures were taken using a microscopy system (Zeiss, Carl Zeiss Jena, Germany). The population doubling time was calculated as the average duration time needed for CD133$^+$ cells to expand to the next generation.

Neural Differentiation Assays of CD133$^+$ Cells in Vitro

Neural differentiation protocols were performed as previously described with slight modifications[47–49]. Cells were plated on PLL- and laminin-coated (Gibco) 24-well coverslips at 10,000 cells/well and cultured for 14 days in neurobasal medium supplemented with 50×B27 and 100×N2 (Invitrogen), 20 ng/ml epidermal growth factor, 20 ng/ml basic fibroblast growth factor (PeproTech) and either free serum or 10% FBS to induce neuronal or glial cell differentiation, respectively.

Gene Expression Profiles of Neurotrophic Factors

Real-time quantitative polymerase chain reaction (RT-qPCR) was performed as previously described[50] to explore the gene expression of neurotrophic factors including NGF, BDNF, GDNF and CNTF on CD133$^+$ cells. Briefly, freshly isolated CD133$^+$ cells, CD133$^-$ cells and BMNCs were harvested and suspended in TRIZOL reagent (Sigma-Aldrich) to extract total RNA according to manufacturer's instructions, and total RNA was then quantified with a spectrophotometric instrument (NanoDrop). Reverse cDNA transcription of 1 μg RNA was performed using a PrimeScript RT Reagent Kit (Takara, Takara Biotechnology (Dalian) Co., Ltd., Liaoning, China) according to manufacturer's descriptions. RT-qPCR was conducted using a CFX96 RT-PCR System (Bio-Rad, Hercules, CA, USA) based on a SYBR Green qPCR Mix (Dongsheng Biotech Co., Ltd., Guangzhou, China) according to manufacturer's instructions. The genes of interest and a reference gene (β-actin) were simultaneously analyzed on the same cDNA sample. Relative expression was calculated by the $2^{-\Delta\Delta C(t)}$ method. The primer sequences of factors above were described previously[27] and purchased from Sangon Biotech (Sangon Biotech Co., Ltd., Shanghai, China).

Labeling of CD133$^+$ Cells

CD133$^+$ cells were transfected with lentiviruses containing the cDNA encoding enhanced green fluorescent protein (EGFP; GeneChem, Shanghai, China) according to manufacturer's instructions. Briefly, cells were seeded at 1×10^5 cells/cm^2 and cultured for 72 h at 37°C in a humidified atmosphere containing 5% CO_2. The cells were visualized with a fluorescence microscope (Zeiss), and the purity was determined by flow cytometry before transplantation.

Transplantation of CD133$^+$ Cells

On day 28 post-STZ injections, mice from the STZ group were randomly selected to receive an intravitreal administration of EGFP-labeled CD133$^+$ cells (1×10^5 in 1 μl) in the right eye, whereas phosphate-buffered saline (PBS; 1 μl) was administered to the left eye. The mice were lightly anesthetized with an i.p. injection of 1% pentobarbital sodium (50 mg/kg) and topically anesthetized with a drop of

oxybuprocaine. The injection was carefully and slowly administered using a 33-gauge syringe (Hamilton Storage, Franklin, MA, USA) into the vitreous body through the pars plana. The untreated mice from the STZ group and age-matched mice from the vehicle group served as controls. All mice were then tested as follows on the 28th and 56th day post-transplantation (Post-D28 and Post-D56).

ERG Recording

The procedures were performed as described previously[27,51–53]. Briefly, mice (n=12 eyes per group on Post-D28 and n=10 eyes per group on Post-D56) were dark-adapted overnight for recording under dim red light. After anesthetization, mice were kept warm on a heating pad maintained at 37°C; the pupils were dilated with one drop of phenylephrine and accommodation blocked with one drop of tropicamide. The ERG responses from both eyes were simultaneously recorded between a gold corneal recording electrode and stainless-steel scalp reference electrodes with a 0.1–300 Hz bandpass filter, while oscillatory potential (OP) responses were recorded with a 70–300 Hz bandpass filter at flash intensity 0.5 log ($cd{\cdot}s{\cdot}m^{-2}$;0 dB). The sum of OP amplitude ($\sum$OPs) was expressed as the sum of the first four OPs (OP1–OP4). The recordings were made using Roland Electrophysiological Systems hardware (Brandenburg, Germany) and a Reti-scan system (Roland Consult, Havel, Germany).

Optomotor Response for Visual Acuity

The procedures were performed as described previously[54,55] and illustrated later in Fig. 3C. Dark-adapted mice (n=12 eyes per group on Post-D28 and n=10 eyes per group on Post-D56) were prepared overnight and placed on the platform at the center of a chamber composed of three computer monitors displaying waves with varied spatial frequency (0.05–0.5 cycle/degree) under scotopic conditions. The mice were habituated for 2 minutes with a gray visual display at the beginning. The rotation speed (12°/s) and contrast (100%) were kept constant. The visual acuity was determined as the highest special frequency based on the observation of head-tracking movements consistent with directions of the stimulus by two individual observers. The right and left eyes were distinguished by their differential sensitivity to anti-clockwise and clockwise rotations, respectively as described previously[54].

Immunofluorescence Analysis

Tissue or cell preparations and immunofluorescence staining were performed as previously described[27,47,50]. For immunofluorescence histochemistry, the eyes (n=5 eyes per group at each time point) were extracted after mice were sacrificed and then prefixed in 4% paraformaldehyde (PFA) at room temperature for 30 min. The anterior segments were then removed using a microscope (Olympus) and fixed in 4% PFA for an additional 2 hours. Subsequently, the eyes were prepared for either frozen sections or whole mounts. For frozen sections, eyes were infiltrated with 30% sucrose overnight at 4°C and then embedded with the optimal cutting temperature (Sakura). Subsequently, 10-μm-thick sections were cut in the sagittal plane using a freezing microtome (Leica, Leica Biosystems, Shanghai, China). For whole mounts, retinas were dissected into four equal parts from the optic nerve (OPN) to peripheral retina and flattened onto glass slides. For immunofluorescence cytochemistry, cells were plated on pre-coated coverslips and then fixed with 4% PFA. After preparation, the samples were incubated with 3% bovine serum albumin and 0.3% Triton X-100 (Beyotime, Shanghai, China) followed by primary antibodies (Table 1) overnight at 4°C and then with fluorophore-conjugated secondary antibodies (Table 1) at 37°C for 1 hour. The retinal capillaries were stained with isolectin GS-IB4 from *Griffonia simplicifolia* (5 μg/ml, Alexa Fluor®568, Life Technology, Grand Island, NY, USA). Nuclei were counterstained with 4',6-diamidino-2-phenylindole (DAPI; Sigma-Aldrich). Confocal images were obtained using a confocal microscopy system (Zeiss LSM 800).

Quantitative Analysis of Histochemistry

The survival and differentiation of transplanted cells were assessed by cell counts as previously described[54,56] with a little modification. Retinal sections were counterstained with DAPI to highlight the different layers of the retina. The nuclei of the transplanted cells (green) were used to define the cell bodies and the location in retina. The number of transplanted cells was determined by counting all $EGFP^+$ cells in serial retina sections. Eyes were excluded from analysis if there was an absence of cells in the vitreous cavity (VC) or the presence of cells sub-retinally. For neural differentiation analysis of transplanted cells co-stained with βIII-tubulin (Tuj1), the number of $EGFP^+Tuj1^+$ cells was quintupled with the average number of $EGFP^+Tuj1^+$ counted in every 5th retina section stained with Tuj1. The cell counting of either $EGFP^+$ cells or $EGFP^+Tuj1^+$ cells was performed on four eyes per group at each time point.

For quantification of retina layer thickness, all measures were made manually on retina section images using ZEN software (Zeiss). Images were taken at the same distance from the midperipheral regions (150–200 μm from the optic disk) at ×20 magnification as before[53]. Retinal sections were counterstained with DAPI to highlight the different layers of the retina. The thickness of individual retina layer was determined as described previously[55], and was averaged for three eyes per group. The number of cells in the ganglion cell layer (GCL) was counted with DAPI showing the nuclei, and was averaged to the number of cells per 100 μm for at least three eyes per group. In some experiments, quantification of number and the length of dendrites and axons of RBCs identified with protein kinase alpha (PKCα) were performed.

Table 1. List of the antibodies.

Name	Application	Host	Supplier
Primary antibodies			
CD133/prominin-1	IF (1:200)	Rat	eBioscience
GFP	IF (1:500)	Chicken	Abcam
PKCα	IF (1:500), WB (1:1000)	Rabbit	Abcam
Tuj1	IF (1:500), WB (1:1000)	Mouse	Sigma
GFAP	IF (1:500)	Rabbit	Abcam
BDNF	IF (1:200)	Rabbit	Abcam
β-Actin	WB (1:1000)	Mouse	Bioworld
Secondary antibodies			
anti-rat IgG Alexa Fluor®488	IF (1:500)	Rabbit	Thermo Fisher Scientific
anti-chicken IgY Alexa Fluor®488	IF (1:1000)	Goat	Thermo Fisher Scientific
anti-mouse IgG Alexa Fluor®568	IF (1:500)	Goat	Thermo Fisher Scientific
anti-rabbit IgG Alexa Fluor®568	IF (1:500)	Goat	Thermo Fisher Scientific
anti-mouse IgG Alexa Fluor®647	IF (1:1000)	Goat	Thermo Fisher Scientific
anti-rabbit IgG Alexa Fluor®647	IF (1:1000)	Donkey	Thermo Fisher Scientific
anti-mouse IgG HRP	WB (1:2000)	Goat	Boster
anti-rabbit IgG HRP	WB (1:2000)	Goat	Boster

BDNF: brain-derived neurotrophic factors; GFAP: glial fibrillary acidic protein; GFP: green fluorescent protein; HRP: horseradish peroxidase; IF: immunofluorescence; Ig: immunoglobulin; WB: Western blotting.

Measurement of the length of dendrites and axons of RBCs has been described previously[57].

For the fluorescence intensity measures of BDNF, mean intensity pixels with BDNF label after subtracting background in images were obtained using ImageJ software (National Institutes of Health, Bethesda, MD, USA) as previously described[58]. Each image was evaluated with uniform rectangle areas (at least three areas per image) to obtain the mean intensity pixels. The intensity values were then averaged for at least five images from three eyes per group.

Western Blotting

Western blotting was performed as previously described[47]. The retinas (n=3 eyes per group at each time point) were lysed in an ice-cold mixture of radioimmunoprecipitation assay (RIPA) buffer and proteinase inhibitor (Beyotime, Shanghai, China) and the concentration was measured using the bicinchoninic acid assay (Beyotime). A total of 20 μg of protein were separated using 10–12% sodium dodecyl sulfate polyacrylamide gel electrophoresis (SDS-PAGE, Beyotime) and transferred onto polyvinylidene fluoride membranes (Bio-rad). The membranes were blocked with Tween-20 Tris-buffered saline (12.5 mM Tris-HCl, pH 7.6,75 mM NaCl and 0.1% Tween-20 [Beyotime, Shanghai, China]) containing 5% fat-free milk for 1 h at room temperature and incubated with primary antibodies (Table 1) over night at 4°C and then with peroxidase-conjugated secondary antibodies (Table 1) for 1 h at room temperature. Chemiluminescent results were detected using the Odyssey infrared imaging system (LICOR Biosciences, Lincoln, NE, USA) and analyzed using ImageJ software (National Institutes of Health, Bethesda, MD, USA) with β-actin as an internal control.

Statistical Analysis

All experiments were individually repeated at least three times. Statistical analysis was performed using SPSS 22.0 (Chicago, IL, USA). Data were presented as the mean ± standard error of the mean (SEM) and plotted with GraphPad Prism 6.0c. Student's two-tailed t tests were used to compare differences between two samples. One-way analysis of variance (ANOVA) followed by Tukey's protected least-significant difference post-hoc test was used for multiple comparisons. Differences were accepted as significant at $P<0.05$.

Results

Isolation and Expansion of Mouse Bone Marrow $CD133^+$ Stem Cells

To determine whether CD133 (prominin-1) selection was useful for bone marrow stem cells, flow cytometry analysis was performed, and the results showed that the percentage of $CD133^+$ cells in mouse BMNCs was $8.78 \pm 4.63\%$ (Fig. 1A). $CD133^+$ cells were then immunomagnetically isolated at a purity of approximately $93.23 \pm 1.05\%$ (Fig. 1B). Immunofluorescence staining verified that these isolated cells expressed CD133 (Fig. 1C).

Flow cytometry was then performed to analyze the expression of bone marrow stem/progenitor phenotypes in freshly isolated $CD133^+$ cells (Fig. 1D). Fresh $CD133^+$ cells expressed high levels of the hematopoietic lineage marker CD45 ($90.17 \pm 4.01\%$), the HSC/HPC markers CD117 ($75.21 \pm 2.61\%$) and CD34 ($24.26 \pm 21.43\%$), and the endothelial line markers CD31 ($24.59 \pm 5.60\%$) and CD309 ($11.53 \pm 1.42\%$), low levels of chemokine receptor CD184 ($6.04 \pm 6.09\%$) and the immunosuppressive marker

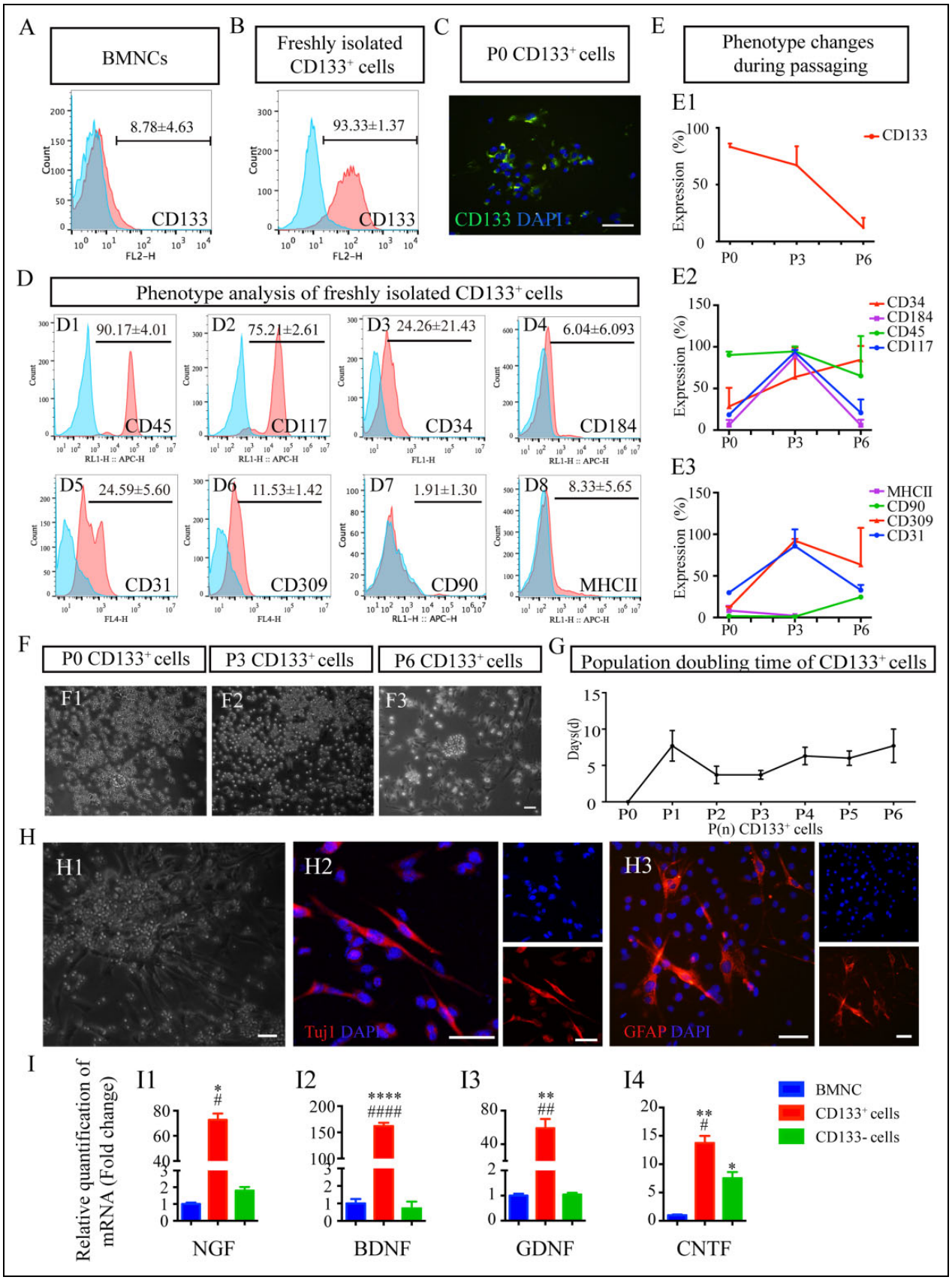

Fig. 1. Isolation and characterization of mouse bone marrow-derived CD133$^+$ stem cells. (A, B) Flow cytometry analysis of the ratio of CD133$^+$ cells (red) (A) before isolation in whole BMNCs and (B) the purity after isolation, compared with isotype control (blue) (n=6).

MHC II (8.33 ± 5.65%), and were negative for MSC marker CD90. These data demonstrated that $CD133^+$ cells represented a hematopoietic/endothelial progenitor fraction in bone marrow.

Since $CD133^+$ cells account for a small fraction in BMNCs, expansion of these cells is needed before transplantation[39]. After sorting, the positive cells were plated and cultured to expand. To determine the relatively optimal generations of cultured $CD133^+$ cells, expanded $CD133^+$ cells were synchronously evaluated the above-described phenotypes (Fig. 1E) and growth characteristics (Fig. 1F and G) in vitro. Expanded $CD133^+$ cells gradually lost their specific marker of CD133 (Fig. 1E1) before the third passage (P3: 67.07 ± 16.68%) and rapidly after then (P6: 12.14 ± 8.72%). Moreover, the expression level of CD45 (Fig. 1E2) was decreased, whereas the expression of CD34 (Fig. 1E2) increased after passaging. Markers including CD117, CD184 (Fig. 1E2), CD31, and CD309 (Fig. 1E3) reached highest expression in P3 $CD133^+$ cells and then declined afterwards, whereas MHC II (Fig. 1E3) reached lowest expression in P3 $CD133^+$ cells and then increased afterwards. Intriguingly, expanded $CD133^+$ cells acquired expression of CD90, which was not present at the moment of isolation, after passaged six times (P6: 24.60 ± 6.58%; Fig. 1E3).

We then investigated the morphological changes (Fig. 1F) and population doubling time (Fig. 1G) of $CD133^+$ cells from different passaging times and found that the cells, when first plated, exhibited the morphology of two populations: a large number of round non-adherent cells with small cell clusters and a small number of adherent cells with pseudopodia (Fig. 1F1). These cells retained their morphologic features (Fig. 1F2) and were passaged relatively rapidly until P6 (Fig. 1G). In P6 cells, when the cultured cells had largely lost expression of CD133, CD117, CD184, CD31, CD309, and acquired expression of CD90 (Fig. 1E), most of cells were adherent and polymorphic (Fig. 1F3).

These data demonstrated that $CD133^+$ cells changed their intrinsic stem/progenitor characteristics over time in culture. In term of phenotype alterations (Fig. 1E) and related growth characteristics (Fig. 1F and G) of expanded $CD133^+$ cells, cells passaged no more than three times, which showed: (1) relatively minimal loss of CD133 phenotype; (2) relatively higher expression of hematopoietic/endothelial progenitor and chemokine receptor phenotypes; (3) relatively lower expression of immunosuppression marker; and (4) a relatively rapid expansion rate, were used in the following experiments.

Characterization of $CD133^+$ cells: The Capacities of Neural Differentiation and Gene Expression of Neurotrophic Factors

Previous studies have demonstrated that the CD133 phenotype is expressed on neural stem/progenitor cells[59], and $CD133^+$ cells from human bone marrow can differentiate to neural lineage cells in vitro[60]. To confirm this, the cells were seeded under the corresponding differentiation conditions. After being cultured for 14 days in neural medium, the cells altered their shape and formed colonies with round cells surrounded by adherent cells that spread radially (Fig. 1H1). Immunofluorescence staining showed that they acquired expression of the neural phenotypes including neuron marker βIII-tubulin (Tuj1; Fig. 1H2) and glial marker glial fibrillary acidic protein (GFAP; Fig. 1H3).

Bone marrow stem/progenitor cells have been documented to secrete a broad range of neurotrophic factors for cell survival and regeneration[21]. Apart from the neural differentiation potential, $CD133^+$ cells have been reported to express a broad range of trophic factors including neurotrophic factors[38,39]. To clarify the neurotrophic effects of $CD133^+$ cells in vitro, RT-qPCR was first performed to investigate gene expression of neurotrophic factors in $CD133^+$ cells (Fig. 1I). $CD133^-$ cells and BMNCs served as controls. The mRNA

Fig. 1. (Continued). (C) Immunofluorescent staining showed freshly isolated $CD133^+$ cells (defined as passage 0; P0) were positive for CD133 (green). DAPI (blue) was used to visualize cell nuclei. (D) Flow cytometry analysis displayed expression of (D1) CD45 (90.17 ± 4.01%, n=4), (D2) CD117 (75.21 ± 2.61%, n=3), (D3) CD34 (24.26 ± 21.43, n=3), (D4) CD184 (6.04 ± 6.093%, n=3), (D5) CD31 (24.59 ± 5.60%, n=3), (D6) CD309 (11.53 ± 1.42%, n=3), (D7) CD90 (1.91 ± 1.30%, n=4), and (D8) MHC II (8.33 ± 5.65%, n=3) in the freshly isolated $CD133^+$ cells after gated $CD133^+$ cells. The isotype control is represented by blue while a shift was represented by red. (E) Plots summarizing the changes over time of phenotypic markers above including (E1) CD133, (E2) CD45, CD117, CD34, CD184, (E3) CD31, CD309, CD90 and MHC II in freshly isolated (P0) and cultured $CD133^+$ cells passaged three (P3) and six (P6) times. (F) Phase-contrast images showing the typical morphology changes of cultured $CD133^+$ cells from (F1) P0, (F2) P3, and (F3) P6. (G) Representative line graph showing population doubling time plotted as the average days needed for the growth of $CD133^+$ cells to next generation. (H) In vitro, $CD133^+$ cells cultured in differentiation media for 14 days (H1) and stained with neural marker (H2) βIII-tubulin (Tuj1; red) and (H3) glial marker GFAP (red) and counterstained with DAPI (blue). (I) Gene expression profiles of neurotrophic factors in $CD133^+$ cells compared with $CD133^-$ cells and BMNCs by RT-qPCR, including (I1) NGF, (I2) BDNF, (I3) GDNF, and (I4) CNTF (n=3). Each mRNA expression of $CD133^+$ cells and $CD133^-$ cells was normalized to the mRNA expression level in BMNCs. The expression level was gated by the black line and represented by mean percentage ± SEM (A, B, D). The plot was generated by mean percentage ± SEM (E, G, I). Statistical analysis: one-way analysis of variance followed by Tukey's multiple comparisons test for (I). *P<0.05, **P<0.01, ****P<0.0001 compared with BMNC in (I). $^{\#}P$<0.05, $^{\#\#}P$<0.01, $^{\#\#\#}P$<0.001, $^{\#\#\#\#}P$<0.0001 compared with $CD133^-$ cells in (I). Scale bars represent 50 μm (C, F, H).

BDNF: brain-derived neurotrophic factor; BMNC: bone marrow mononuclear cell; CNTF: ciliary neurotrophic factor; DAPI: 4′,6-diamidino-2-phenylindole; GDNF: glial cell-derived neurotrophic factor; GFAP: glial fibrillary acidic protein; MHC: major histocompatibility complex; NGF: nerve growth factor; RT-qPCR: real-time quantitative polymerase chain reaction; SEM: standard error of the mean.

expression level was normalized to those in BMNCs as 1. Significance was found among three groups. We observed significant increases in the mRNA levels of NGF (Fig. 1I1; 73.8-fold versus 1.8-fold change; $P<0.05$), BDNF (Fig. 1I2; 161.9-fold versus 0.7-fold change; $P<0.0001$), GDNF (Fig. 1I3; 59.1-fold versus 1.0-fold change; $P<0.01$), and CNTF (Fig. 1I4; 13.8-fold versus 7.5-fold change; $P<0.05$) in $CD133^+$ cells compared with $CD133^-$ cells, respectively. No significance in the mRNA levels of the above factors was found between $CD133^-$ cells and BMNCs except for CNTF (7.5-fold change; $P<0.05$).

These findings demonstrated that bone marrow $CD133^+$ cells were able to differentiate into neuronal-like cells in vitro and express genes of abundant neurotrophic factors. The results further indicated that $CD133^+$ cells had the potential to regenerate or ameliorate neurodegenerative disorders such as DR by cell replacement and support of neural cell survival.

Transplantation of $CD133^+$ Cells Survives and Migrates to the IR in STZ-Induced Diabetic Mice with Early-Stage DR

To test our hypothesis that $CD133^+$ cells can ameliorate neural dysfunction and degeneration at early stage of DR, the DM mouse model was first established by administering a single dose of 150 mg/kg STZ i.p. to adult male C57BL/6 mice. STZ mice displayed significantly higher levels of FBG ($P<0.01$) but lower weight ($P<0.05$) than vehicle mice from the third day after DM induction, and these features were maintained for up to 140 days (Fig. 2B).

In light of previous studies on the development of DR in STZ mice[14,61], early DR neuronal degeneration was identified on D28, D56 and D84 before transplantation (Supplementary Fig. 1) in STZ mice compared with age-matched vehicle mice. STZ-induced diabetic mice experienced progressive changes of early DR over time from D28 after DM induction, which were characterized by significantly reduced scotopic ERG and OPs responses (Supplementary Fig. 1A, C, and D) and IR cell loss, including RGC and RBC degenerations (Supplementary Fig. 1B, E, and F). Therefore, $CD133^+$ cell transplantation was performed on STZ mice on D28 after DM induction. The effect of transplantation was assessed on Post-D28 and Post-D56, as illustrated in Fig. 2A.

Before transplantation, cultured $CD133^+$ cells were labeled with EGFP by lentiviral infection (Fig. 2C) to better evaluate the effect of cell treatments. Three days after transfection, $CD133^+$ cells maintained their morphology (Fig. 2C1) and were labeled with green fluorescence (Fig. 2C2 and C3). Flow cytometry analyses showed that approximately $97.10 \pm 0.28\%$ of the $CD133^+$ cells were labeled with EGFP (Fig. 2C4). We traced transplanted EGFP-labeled $CD133^+$ cells in the retina from STZ+$CD133^+$ group compared with STZ+PBS group on Post-D28 and Post-D56 (Fig. 2D–G). Donor cells were mainly located in the VC (Fig. 2(d)1) and some of them migrated to the GCL (Fig. 2D2 and D3), inner nuclear layer (INL) and inner plexiform layer (IPL) (Fig. 2D2). Approximately 20,000 cells and 7000 cells survived on Post-D28 and Post-D56, respectively, and demonstrated a significantly decreased number of survived $EGFP^+$ cells over time on Post-D56 compared with Post-D28 ($P<0.01$; Fig. 2F). Interestingly, relative decreased percent of cells in the VC (Post-D28 versus Post-D56: 59% versus 44%) and increased percent of cells in the IR, particularly in GCL (Post-D28 versus Post-D56: 14% versus 26%), were observed on Post-D56 compared with Post-D28 (Fig. 2G).

These findings indicated that $CD133^+$ cells, although significantly decreased number of survived cells was observed, could migrated to the IR, particularly GCL, in STZ-induced diabetic mice during the post-transplantation period.

Transplantation of $CD133^+$ Cells Prevents Early Visual Dysfunction in STZ-induced Diabetic Mice with Early-Stage DR

We then tested the effect of $CD133^+$ cells on visual function in STZ mice after transplantation. The impaired electrical responses of the retina associated with DR have been reported and are related to disease progression[7]. In line with this finding, STZ mice were identified to be involved in DR at the early stage before transplantation on D28 (Pre-D0) with ERG and OPs recordings (Fig. 3A and B). Significance was observed among four groups (ANOVA: $P<0.05$) on Post-D28 and Post-D56 (Fig. 3B). After STZ injection, eyes from either STZ-untreated or STZ+PBS group showed a significant decrease in the amplitude of the scotopic a-wave (Fig. 3B1) and b-wave (Fig. 3B2) compared with vehicle group on Post-D28 and Post-D56. Transplantation of $CD133^+$ cell significantly increased the scotopic b-wave amplitude until Post-D56 (Fig. 3B2; ANOVA: $P<0.0001$ among four groups; STZ+PBS versus STZ+$CD133^+$: 232.69 ± 27.3 μV versus 339.3 ± 24.9 μV on Post-D28, and 222.9 ± 19.3 μV versus 305.2 ± 23.3 μV on Post-D56; $P<0.05$). Although there was no significance in the a-wave amplitude between the STZ+$CD133^+$ and STZ+PBS groups, the retina from STZ+$CD133^+$ showed relatively improved a-wave response, with no significant difference detected between the STZ+$CD133^+$ group and the vehicle group on Post-D56 (Fig. 3B1). Increased amplitude of $\sum$OPs was also observed in the STZ+$CD133^+$ group after transplantation, with statistical significance on Post-D28 but not on Post-D56 (Fig. 3D3; ANOVA: $P<0.001$; STZ+PBS versus STZ+$CD133^+$: ΣOPs: 129.0 ± 7.0 μV versus 167.3 ± 16.0 μV on Post-D28 with $P<0.05$ and 118.6 ± 10.5 μV versus 134.0 ± 9.6 μV with $P>0.05$). No significance was found between STZ-untreated and STZ+PBS group.

In addition, impairment of visual acuity has been detected in both human and animal models with early DR[62] (Fig. 3C

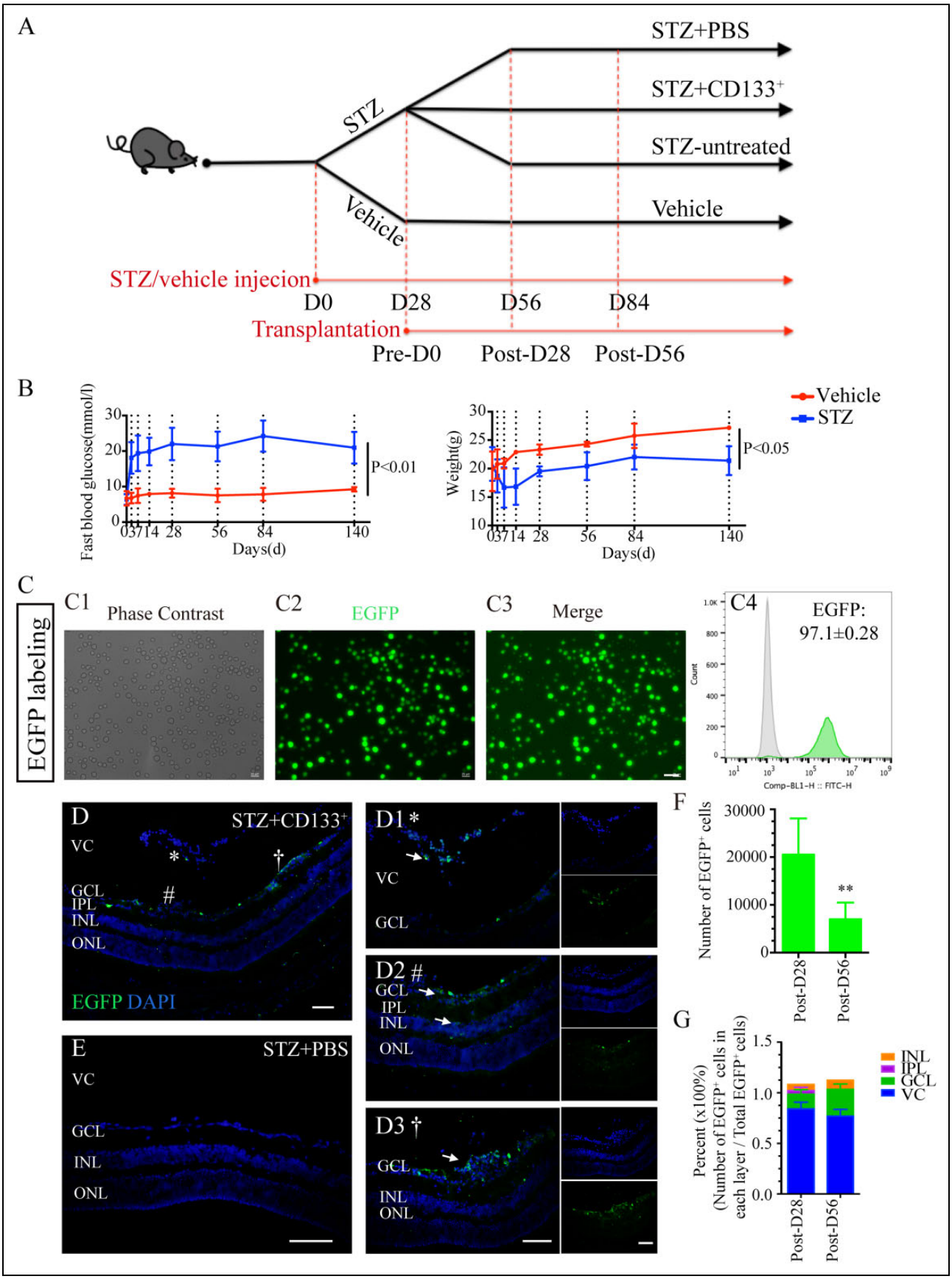

Fig. 2. Transplanted CD133^{+} cells survive and migrate in STZ-induced diabetic retina with early DR. (A) Chronological diagram of design for animal grouping: 8-week-old C57BL/6 adult male mice were injected i.p. with either 150 mg/kg STZ (STZ group) or citrate buffer (vehicle

and D). In line with the impaired ERGs above, reduced visual acuity based on the scotopic optomotor responses was also observed in STZ mice. Significance was found among four groups (Fig. 3D; ANOVA: $P<0.0001$ on Post-D28 and $P<0.001$ on Post-D56). After the treatment with $CD133^+$ cells, increased visual acuity was found up to 56 days post-transplantation (Fig. 3D; STZ+PBS versus STZ+$CD133^+$: 0.36 ± 0.05 cycles/degree versus 0.48 ± 0.02 cycles/degree on Post-D28 with $P<0.01$ and 0.36 ± 0.02 cycles/degree versus 0.48 ± 0.04 cycles/degree with $P<0.05$). No significance was found between STZ-untreated and STZ+PBS group.

These data suggested that $CD133^+$ cell transplantation prevented visual dysfunction in STZ mice in both retinal and post-retinal layers for at least 28 days post-transplantation, resulting in better visual performance up to 56 days post-transplantation.

Transplanted $CD133^+$ Cells Preserve Diabetes-Induced IR Thickness Thinning in STZ Mice

Previous studies have demonstrated that a decreased thickness of the IR layer contributes to a decreased thickness of total retina (TR) layers and is related to neuroretinal dysfunctions[7,13]. To study the histological changes in the retina associated with the functional results above, we performed retina thickness measurements among four groups (Fig. 4A), including thickness of TR, IR, IPL, INL, outer plexiform layer (OPL) and outer nuclear layer (ONL), and number of cells in GCL per 100 μm (Fig. 4B). Significant differences were found among four groups (Fig. 4B) except for the thickness of the ONL (Fig. 4B7; ANOVA: $P>0.5$). After DM induction with STZ, retinas from STZ mice were found to have a reduced cell number in the GCL and the thickness of the individual layers above except for the ONL (Fig. 4B). Transplantation of $CD133^+$ cells significantly suppressed these changes including the IR (Fig. 4B2; STZ+PBS versus STZ+$CD133^+$: 51.80 ± 3.27 μm versus 66.98 ± 3.30 μm on Post-D56; $P<0.01$), GCL (Fig. 4B3; STZ+PBS versus STZ+$CD133^+$: 30.75 ± 10.07/100 μm versus 23.69 ± 5.26/100 μm on Post-D56; $P<0.01$), IPL (Fig. 4B4; STZ+PBS versus STZ+$CD133^+$: 26.66 ± 2.08 μm versus 35.05 ± 2.33 μm on Post-D56; $P<0.05$), INL (Fig. 4B5; STZ+PBS versus STZ+$CD133^+$: 30.75 ± 10.07 μm versus 23.69 ± 5.26 μm on Post-D56; $P<0.05$), OPL (Fig. 4B6; STZ+PBS versus STZ+$CD133^+$: 11.12 ± 0.56 μm versus 14.33 ± 0.36 μm on Post-D56; $P<0.01$), but not ONL (Fig. 4B7) up to 56 days post-transplantation. There was no significant difference in TR thickness when comparing STZ+$CD133^+$ group with either STZ+PBS or vehicle group on both Post-D28 and Post-D56 (Fig. 4B1).

These data demonstrated that, considering the results of cell survival in IR in Fig. 2, transplantation of $CD133^+$ cells were able to suppress diabetes-induced thinning of the IR thickness.

$CD133^+$ Cell Transplantation Prevents Diabetes-Induced RGC and RBC Degeneration in the IR

The early ERG findings in DR strongly suggest that dysfunction begins in the neurons of the IR[7]. The loss of RGCs and RBCs has been reported in diabetes[15] and was detected to occur from D28 post-STZ in our study (Supplementary Fig. 1B, E, and F). Considering functional and histological results above after transplantation of $CD133^+$ cells including preserved functions of b-wave and OPs (Fig. 3A and B), as well as the thickness of the GCL, IPL, INL and OPL (Fig. 4), RGCs and RBCs changes were analyzed on Post-D28 (Fig. 5A–E) and Post-D56 (Fig. 5F–J) by immunofluorescence staining. Immunolabeling of RGCs and RBCs was performed with Tuj1 and PKCα markers after $CD133^+$ cell transplantation. Immunofluorescence staining of retina sections from four groups showed that the retinas of the STZ-untreated or STZ+PBS group displayed less expression of Tuj1 (Fig. 5B and G) and PKCα (Fig. 5A and F) compared with retinas from the vehicle group. After $CD133^+$ cell

Fig. 2. (Continued). group). Eyes of STZ mice were further assigned into STZ+133^+ group, STZ+PBS group, and STZ-untreated group. The day injected was regarded as D0. The day of D28 before transplantation was regarded as Pre-D0. The day on the 28th and 56th day after transplantation were regarded as Post-D28 and Post-D56, respectively. Animal experiments were performed on D28 (Pre-D0), D56 (Post-D28) and D84 (Post-D56). (B) Line graphs showing the FBG levels and weight changes within experimental time comparing STZ diabetic mice (blue line) with vehicle mice (red line) within experimental time ($n=10$ mice per group for each time point). (C) Cultured P3 $CD133^+$ cells were labeled with EGFP (green) before transplantation. Representative images showing green fluorescence labeled cells under the (C1) phase-contrast, (C2) EGFP, and (C3) merge images after incubation with EGFP-loaded lentiviruses for 5 days. (C4) Flow cytometry analysis showing the purity of $EGFP^+CD133^+$cells (green) compared with non-labeled $CD133^+$cells (gray). (D, E) Representative images of survival and migration of intravitreally transplanted EGFP-labeled $D133^+$ cells (green) from (D) STZ+$CD133^+$ group retina compared with (E) STZ+PBS retina on the 28th (Post-D28) and 56th (Post-D56) day after transplantation ($n=4$ eyes per group). (D1–D3) Zoom-in images in (B) display transplanted $CD133^+$($EGFP^+$; green) cells mainly (D1) located in VC and (D2, D3) some of them migrated into GCL and IR. *, # and † represent the location of images taken and zoom-in in (D1), (D2) and (D3), respectively. (F) Histogram showing the number of $CD133^+$ cells ($EGFP^+$; green) found on Post–D28 and Post–D56 in the retina. (G) Histogram showing the percentage of $EGFP^+$ cells found in VC, GCL, IPL, and INL compared with total $EGFP^+$ cells on Post-D28 and Post-D56, respectively. The expression level in (C4) is gated by the black line and represented by mean percentage ± SEM. Values expressed as mean ± SEM. White arrows indicate transplanted cells. Statistical analysis: Student's *t* test for (B, F). **: $P<0.01$. Scale bars represented 50 μm (C, D, E).

DR: diabetic retinopathy; EGFP: enhanced green fluorescent protein; FBG: fasting blood glucose; GCL: ganglion cell layer; INL: inner nuclear layer; i.p.: intra peritoneally; IPL: inner plexiform layer; IR: inner retina; ONL: outer nuclear layer; SEM: standard error of the mean; STZ: streptozotocin; VC: vitreous cavity.

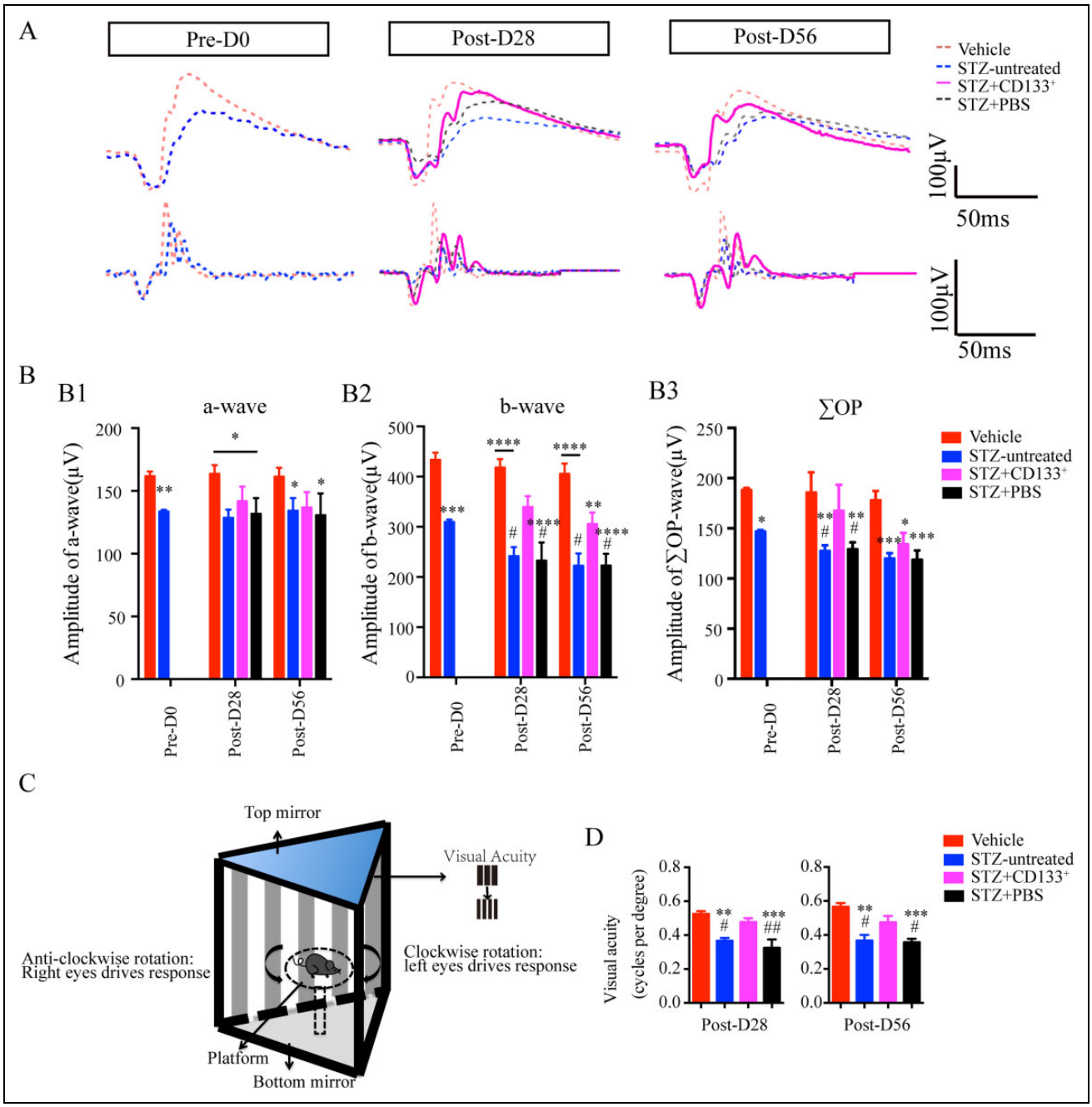

Fig. 3. Intravitreal transplantation of CD133$^+$ cells prevents early visual dysfunction in STZ-induced diabetic mice. (A, B) Transplantation of CD133$^+$ cells improved scotopic ERG responses in diabetic mice especially the b-wave and the sum of oscillatory potentials (∑OPs) up to Post-D56 in diabetic retina. (A) Representative images of scotopic ERG on Pre-D0, Post-D28, and Post-D56 at flash intensity of 0.5 log (cd·s·m^{-2}; 0dB). Upper: ERGs. Bottom: OPs. Red dashed line: vehicle; blue dashed line: STZ-untreated; magenta line: STZ+CD133$^+$; black dashed line: STZ+PBS. (B) Corresponding statistic graphs displaying the amplitude of (B1) a-wave, (B2) b-wave, and (B3) ∑OPs. (C, D) Scotopic optomotor responses assessed by visual acuity via optomotor illustrated in (C) was improved in STZ+CD133$^+$ group up to Post-D56, compared with the other three groups. (D) Measurement of visual acuity from four groups plotted as a histogram. Number of vehicle (red) versus STZ-untreated (blue) versus STZ+CD133$^+$(magenta)/PBS (black) eyes: Pre-P0: n=10 versus 10, Post-D28: n=2 versus 12 versus 12, Post-D56: n=10 versus 10 versus 10. Values expressed as mean ± SEM. Statistical analysis: One-way analysis of variance followed by Tukey's multiple comparisons test for (B) and (D). Compared with vehicle group: *P<0.05, **P<0.01, ***P<0.001, ****P<0.0001; Compared with STZ+ CD133$^+$ group: $^{\#}P$<0.05, $^{\#\#}P$<0.01.

ERG: electroretinogram; OP: oscillatory potential; PBS: phosphate-buffered saline; SEM: standard error of the mean; STZ: streptozotocin.

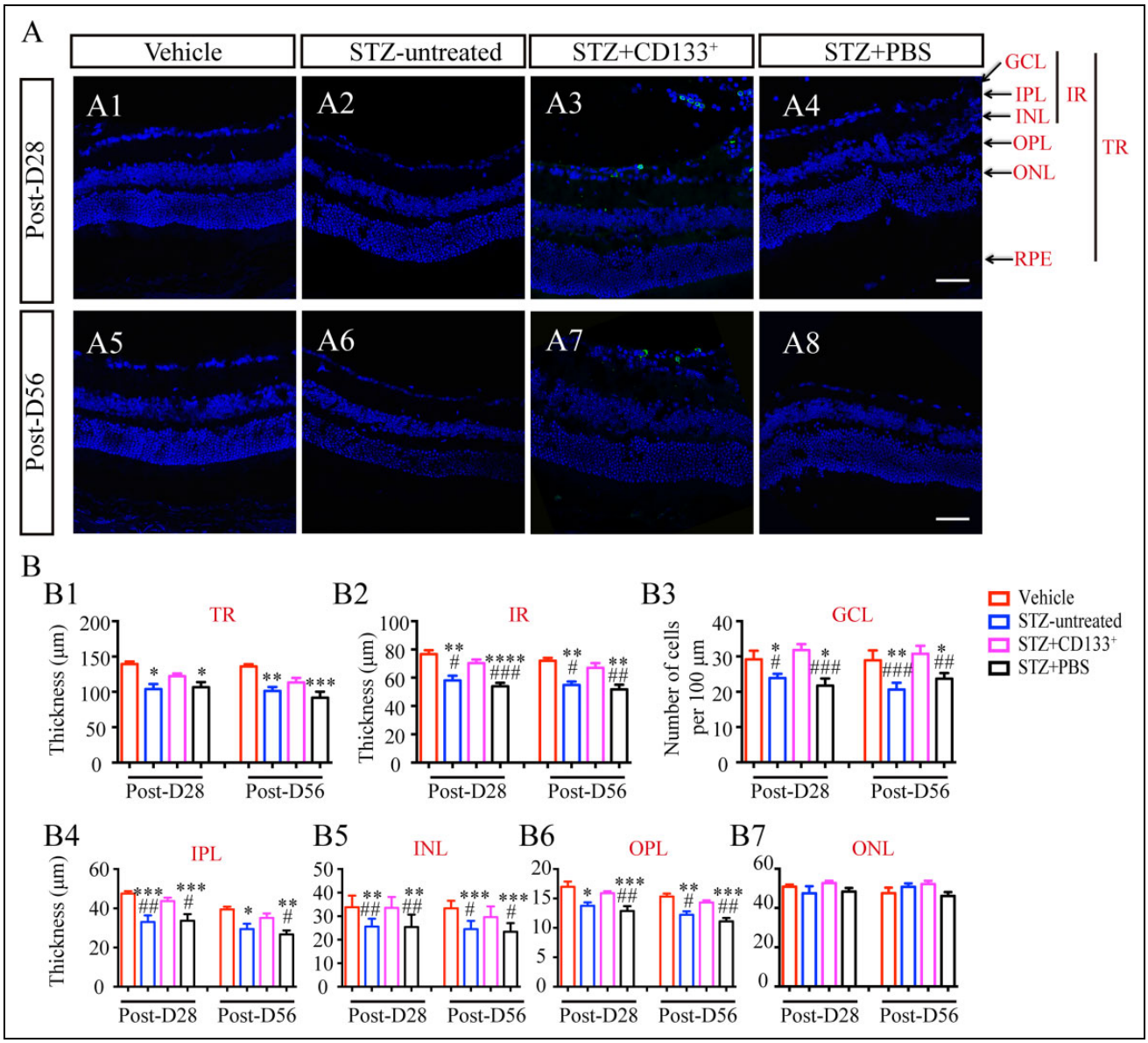

Fig. 4. Transplanted CD133$^+$ cells suppress inner retinal thinning in STZ-induced diabetic mice with early DR. (A) Representative images of retina from vehicle, STZ-untreated, STZ+CD133$^+$, and STZ+PBS group and (B) statistical histograms of thickness of TR, IR and individual retina layers, and number of cells in GCL per 100 μm. CD133$^+$ cells prevented thinning of layers in diabetic mice, especially IR, but not ONL. Values expressed as mean ± SEM (B) (n=4 eyes per group). Statistical analysis: One-way analysis of variance followed by Tukey's multiple comparisons test for (B). Compared with vehicle group: *P<0.05, **P<0.01, ***P<0.001, ****P<0.0001; Compared with STZ+CD133$^+$ group: $^{\#}P$<0.05, $^{\#\#}P$<0.01, $^{\#\#\#}P$<0.001. Scale bars represent 50 μm (A).
DR: diabetic retinopathy; IR: inner retina; GCL: ganglion cell layer; ONL: outer nuclear layer; OPL: outer plexiform layer; PBS: phosphate-buffered saline; RPE: retina pigment epithelium; SEM: standard error of the mean; STZ: streptozotocin; TR: total retina.

transplantation, STZ mice exhibited increased Tuj1 (Fig. 5B and G) and PKCα (Fig. 5A and F) expression in the retina. Western blotting was further performed to quantify the alterations and revealed the same alterations. Significance was found among four groups. After cell transplantation, the relative levels of both PKCα and Tuj1 in STZ+CD133$^+$ group were significantly higher than those in the STZ+PBS group on Post-D28 (Fig. 5D and E; STZ+PBS versus STZ+CD133$^+$: 0.66 ± 0.07 versus 0.94 ± 0.09 for Tuj1 with P<0.05 and 0.63 ± 0.09 versus 0.93 ± 0.11 for PKCα with P<0.05), but not on Post-D56 (Fig. 5I and J). However, no significance was observed between STZ+CD133$^+$ group and vehicle group on Post-D56 (Fig. 5J; STZ+CD133$^+$ group: 0.83 times for Tuj1 and 0.81 times for PKCα compared with vehicle group; P>0.05). We also observed EGFP$^+$CD133$^+$ cells integrated into the GCL (Fig. 5A3, B3, F3, and G3) and some cells co-expressing Tuj1 were aligned with other RGCs in the STZ+CD133$^+$ retina (Fig. 5B3 and G3).

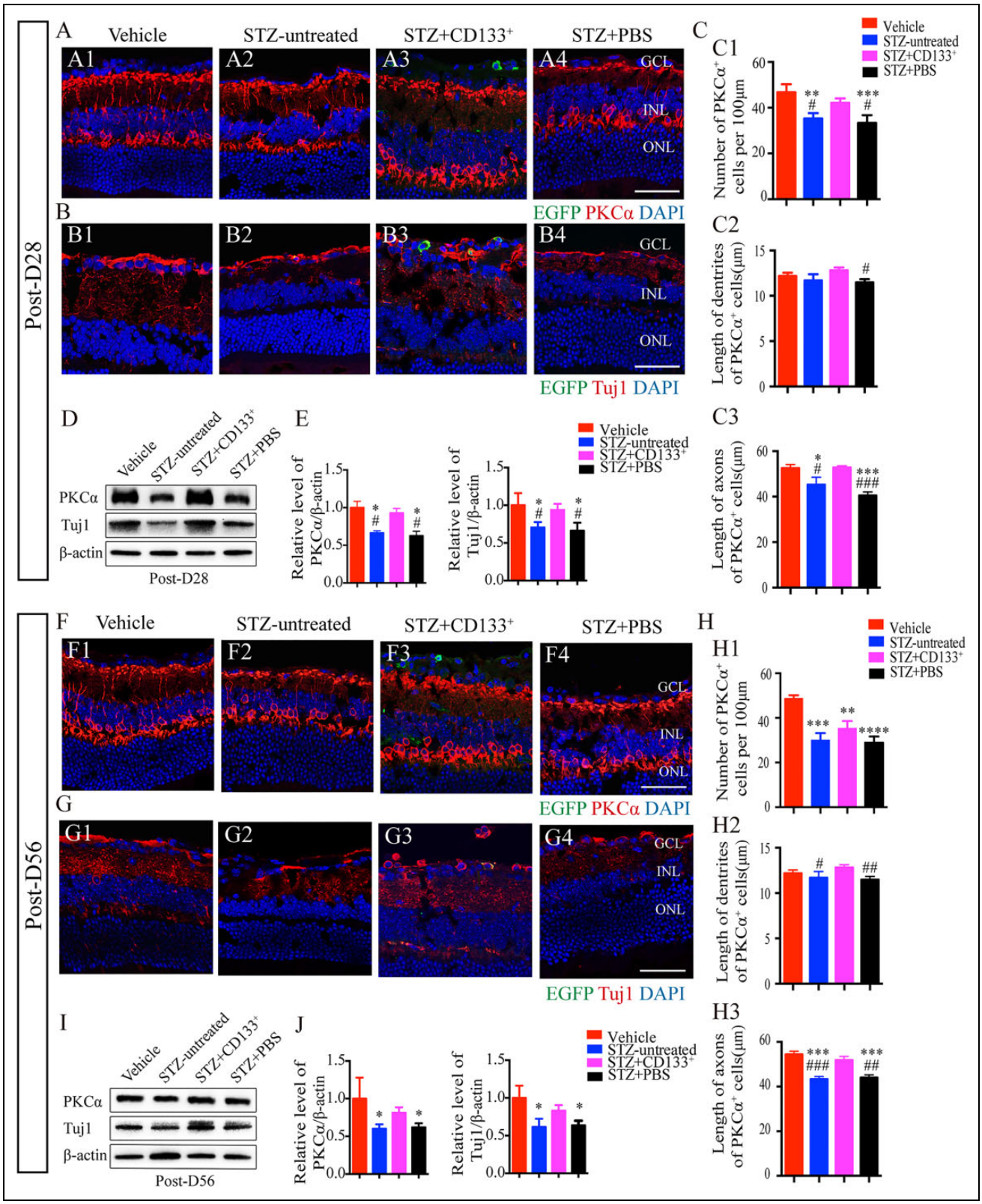

Fig. 5. Transplanted CD133$^+$ cells delay neuronal degeneration in IR in STZ-induced diabetic mice. (A, B, F, G) Representative images showing the rescue of RBCs stained with protein kinase C alpha (PKCα) (red), and RGCs with Tuj1 (red) on Post-D28 and Post-D56 in STZ+CD133$^+$ group mice, respectively (A3, B3, F3, G3), compared with vehicle (A1, B1, F1, G1), STZ-untreated (A2, B2, F2, G2), and STZ+PBS group (A4, B4, F4, G4). Images were taken at the same location among retinas from four groups to make reliable comparisons. (C, H) Histogram showing the number (per 100 μm), dendrite length, and axon length of PKCα$^+$ cells in retina from four groups. Related

In addition, we measured the number and length of dendrites and axons of PKCα-positive cells to study the morphology changes among the four groups, and significance was observed (Fig. 5C and H; ANOVA: $P<0.05$). Significantly reduced numbers and lengths of axons of PKCα-positive cells (Fig. 5C1, C3, H1, and H3) on either STZ-untreated or STZ+PBS mice were found, compared with vehicle on Post-D28 and Post-D56, whereas a shorter length of dendrites was found, but with no significance (Fig. 5C2 and H2). Transplantation of $CD133^+$ cells averted these changes and significantly increased the number and length of axons compared with PBS on Post-D28 (Fig. 5C1 and C3; STZ+PBS versus STZ+$CD133^+$: 33.33 ± 3.40 versus 42.14 ± 1.89 per 100 μm for number with $P<0.05$ and 40.52 ± 1.53 μm versus 52.85 ± 0.70 μm for axon length with $P<0.05$). Significance was found for the length of axons (Fig. 5H3) but not the number on Post-D56 (Fig. 5H1; STZ+PBS versus STZ+$CD133^+$: 44.03 ± 1.28 μm versus 51.87 ± 1.64 μm for the length of axons with $P<0.01$). Although no significance was found regarding the length of dendrites between the STZ group and vehicle group, significantly longer dendrites were found in the cell-treated group than in PBS-treated group on both Post-D28 and Post-D56 (Fig. 5C2 and H2; vehicle versus STZ+PBS versus STZ+$CD133^+$: 12.74 ± 0.51 μm versus 10.67 ± 0.81 μm versus 13.61 ± 0.47 μm on Post-D56). No significance was found between the STZ-untreated and STZ+PBS group.

These data indicated that CD133+ cells could preserve the IR degeneration, including rescuing the RBC and RGC degeneration, at the early stage of DR.

Neural Differentiation and Neurotrophic Potential of Grafted $CD133^+$ cells in STZ-Induced Diabetic Retina

Although we observed that transplantation of $CD133^+$ cells prevented deteriorated function and structure in STZ mice in the early stage of DR, the underlying mechanism remains unclear. The bone marrow contains adult stem cells with the ability to regenerate damaged cells and tissues through cell replacement, trophic support, and immunomodulation[21]. Because we observed the characteristic capacities of neural differentiation (Fig. 1H) and gene expression of neurotrophic factors (Fig. 1I) in $CD133^+$ cells in vitro, further investigations on the possibility of neural differentiation and neurotrophic factor expression were performed in retina sections from four groups.

Immunofluorescence results in Fig. 5B3 and G3 showed that transplanted $CD133^+$ cells migrated to the GCL and expressed Tuj1. Subsequently, we addressed the differentiation capacity of the $CD133^+$ cells in vivo (Fig. 6). The retinas from STZ+$CD133^+$ group were evaluated with immunofluorescence staining and revealed that, some EGFP-labeled $CD133^+$ cells located in the GCL and optic nerve zone (OPN) were able to co-express Tuj1 but not PKCα (Fig. 6A; arrowheads) on both Post-D28 and Post-D56. In line of this, we counted the percentage of $EGFP^+Tuj1^+$ cells in the total $EGFP^+$ cells (Fig. 6B) or cells in the GCL layer (Fig. 6C) over time. There was a decreased percentage of $EGFP^+Tuj1^+$ cells in the total $EGFP^+$ cells on Post-D56 (26%) compared with Post-D28 (13%), and so was the percentage in the GCL (Post-D56 versus Post-D28: 90% versus 70%). We also detected that only scattered $EGFP^+$ cells could co-stain with GFAP (Fig. 6D; arrowheads). Considering the location and migration of $CD133^+$ cells (Fig. 2), increased number of cells in the GCL (Fig. 4), and increased expression of Tuj1 (Fig. 5), we suggested that $CD133^+$ cells might at least contribute to the prevention of RGCs in the GCL.

However, given that the location of transplanted cells was mainly the GCL, the restoration of visual function and IR due to engrafted cell differentiation might not be sufficient. A previous study of human $CD133^+$ cells displayed the ability to induce regeneration by a paracrine effect through correct location to the injured sites[41]. We have addressed gene expression of neurotrophic factors in Fig. 1I and above all, the mRNA level of BDNF was relatively the highest. The loss of neurotrophic factors including BDNF has been reported in diabetes rodents[8]. In line with the previous studies regarding the protective role of BDNF on the survival of the RGCs and RBCs[31,57], we further assessed the expression of BDNF on the retina sections from four groups (Fig. 7A and B). Immunofluorescence staining of BDNF in the retina sections from STZ+$CD133^+$ group on Post-D28 and Post-D56 showed that EGFP-labeled $CD133^+$ cells migrate to the IR (particularly the GCL) and expressed BDNF (Fig. 7A3, A7, and C; arrowheads). Representative images of BDNF labeling in retina sections from four groups are displayed in Fig. 7A on both Post-D28 and Post-D56 and revealed that retinas from STZ+$CD133^+$ group expressed a higher level of BDNF than PBS. Quantification of BDNF label was performed to further demonstrate the difference with normalization to vehicle group at each time point as 1 (Fig. 7B). Significance was found among four groups (ANOVA: $P<0.0001$). After $CD133^+$ cell transplantation, retinas showed a significantly increased level of BDNF labeling compared with either STZ-untreated and PBS group up to

Fig. 5. (Continued). Western blotting is shown in (D, I) and statistical optical density ratio analysis compared with vehicle group (the average value set as 1) in (E, J). β-actin was used as an internal control. Images were representative for at least five images per eye ($n=4$ eyes per group). Values expressed as mean ± SEM ($n=3$ eyes per group). DAPI stained the nuclei. Statistical analysis: One-way analysis of variance followed by Tukey's multiple comparisons test for (E, J, C, H). Compared with vehicle group: $^*P<0.05$, $^{**}P<0.01$, $^{***}P<0.001$, $^{****}P<0.0001$; Compared with STZ+ $CD133^+$ group: $^{\#}P<0.05$, $^{\#\#}P<0.01$, $^{\#\#\#}P<0.001$. Scale bars represent 50 μm (A, B, F, G).

DAPI: 4',6-diamidino-2-phenylindole; PBS: phosphate-buffered saline; RBC: rod-on bipolar cell; RGC: retinal ganglion cell; SEM: standard error of the mean; STZ: streptozotocin.

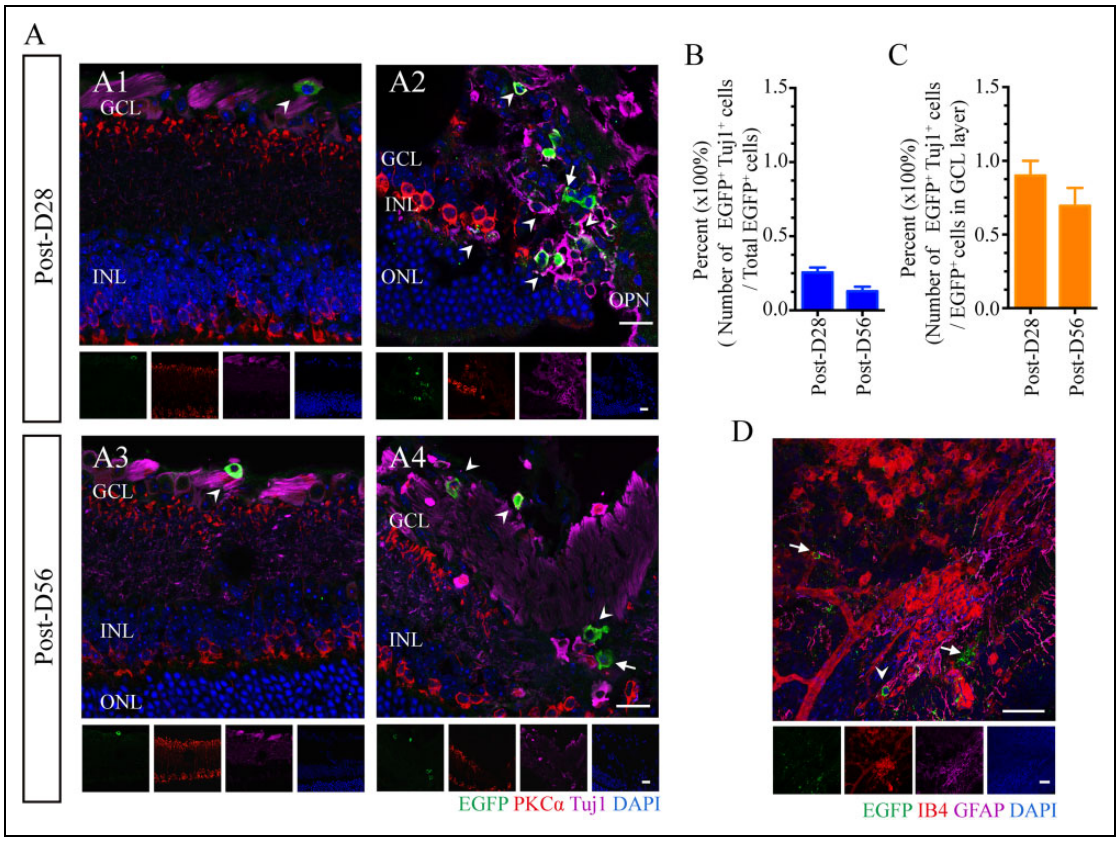

Fig. 6. Neural differentiation ability of CD133$^+$ cells in STZ-induced diabetic mice. (A) Representative images showing intravitreal transplantation of CD133$^+$ (EGFP$^+$; green) cells in diabetic retina were found on Post-D28 and Post-D56, and expressed RGC marker Tuj1 (magenta) but not retina specific RBC marker PKCα (red). (B, C) Corresponding histograms showing the percentage of number of EGFP$^+$Tuj1$^+$ cells versus EGFP$^+$ cells (E) in total and (F) in GCL layer on Post-D28 and Post-D56, respectively. (D) Only scatter CD133$^+$ cells expressed GFAP (magenta). DAPI (blue) in (A, D) show the nuclei. Isolectin B4 (IB4) (red) in (D) show the vessel walls. White arrows indicate EGFP$^+$ transplanted cells and white arrowheads indicate the overlay cells (A, D). Images were representative of six random fields (n=3). Values expressed as mean ± SEM (n=3; B, C). OPN: optic nerve. Scale bars represent 50 μm (D) and 20 μm (A).
DAPI: 4',6-diamidino-2-phenylindole; EGFP: enhanced green fluorescent protein; GFAP: glial fibrillary acidic protein; RBC: rod-on bipolar cell; RGC: retinal ganglion cell; SEM: standard error of the mean.

56 days post-transplantation (Fig. 7B; STZ-untreated versus STZ+PBS versus STZ+CD133$^+$: 0.63 versus 0.65 versus 2.18 times with P<0.0001 on Post-D28 and 0.64 versus 0.56 versus 1.45 times with P<0.01 on Post-D56). Intriguingly, retinas from the STZ+CD133$^+$ group expressed significantly higher level than the vehicle on Post-D28. No significance could be detected between the STZ-untreated and STZ+PBS group. These data demonstrated that, considering increased expression of BDNF in the retina, transplantation of CD133$^+$ cells could preserve visual dysfunction and IR degeneration via increased expression of BDNF in STZ-induced diabetic retina.

Discussion

This study has demonstrated that, if intravitreally introduced early, bone marrow-derived CD133$^+$ stem cells could ameliorate visual dysfunctions in STZ mice by IR protection through 56 days post-transplantation. In the present study, we isolated CD133$^+$ stem cells from the mouse bone marrow and found that they co-expressed phenotypes of HSCs/HPCs and EPCs. The expansion of CD133$^+$ cells under our culture conditions allowed maintenance of their intrinsic stem/progenitor characteristics for up to six passages. In addition, CD133$^+$ cells are able to differentiate into neuronal-like cells and expressed abundant trophic factors genes in vitro. We found that, after intravitreal transplantation in STZ mice, CD133$^+$ cells survived, migrated into the IR and delayed the underlying morphological abnormalities and cell loss in the IR including RGCs and RBCs, which significantly preserve dark-adapted visual functions based on observations including ERG (OPs) and optomotor responses. We further demonstrated the potential mechanisms underlying these cell transplantation effects and found that a subset of transplanted CD133$^+$ cells were able to express the neurotrophic factor of BDNF, and differentiate to express the RGC marker of Tuj1. Moreover, transplantation of these cells

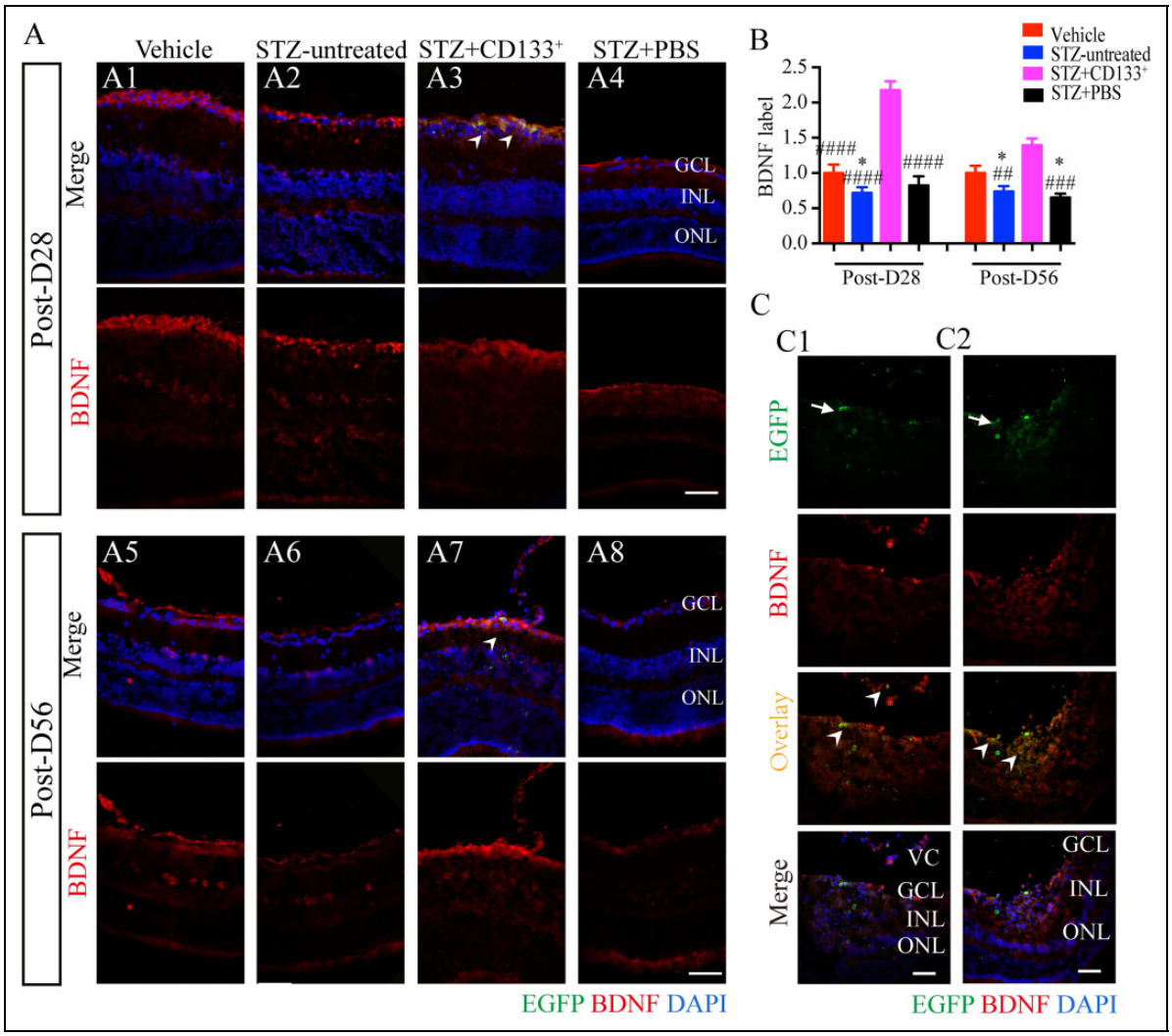

Fig. 7. Neurotrophic potential of CD133$^+$ cells in STZ-induced diabetic retina. (A, B) BDNF staining among four groups on Post-D28 and Post-D56 (A) and relative quantification of BDNF level (B). (C) A subset of transplanted CD133$^+$ cells (green) was localized in VC and GCL and expressed BDNF (overlay; yellow) in STZ+CD133$^+$ retina. Values expressed as mean ± SEM (n=5 per group). White arrows indicate EGFP$^+$ transplanted cells and white arrowheads indicate the overlay cells in (A, C). Statistical analysis: one-way ANOVA followed by Tukey's multiple comparisons test for (B). *P<0.05 compared with vehicle group. ##P<0.01, ###P<0.001, ####P<0.0001 compared with STZ+CD133$^+$ group. Scale bars represent 50 μm (A, C).
BDNF: brain-derived neurotrophic factor; EGFP: enhanced green fluorescent protein; GCL: ganglion cell layer; SEM: standard error of the mean; STZ: streptozotocin; VC: vitreous cavity.

increased expression of BDNF in the STZ retina to protect and support retinal cell survival.

Characterization of Mouse Bone Marrow-Derived CD133$^+$ Stem Cells

CD133/prominin-1 is a well-documented stem cell marker that was discovered in 1997[34]. In the present study, we identified approximately 8.78% of mouse BMNCs expressed CD133, which is in line with the results of a previous study[63]. CD133$^+$ stem cells shared similar phenotypes as those demonstrated in other studies: they were positive for the HSC/HPC markers CD45, CD117, and CD34; the EPC markers CD34 and CD309; and the chemokine marker CD184 but negative for the MSC marker CD90 in humans and mice[38,63].

As CD133$^+$ cells occupy a small fraction in bone marrow, expansion efforts are needed to obtain a sufficient number of cells for experiments[39]. In our study, CD133$^+$ cells did not lose specific expressions of CD133, CD117, CD184, CD45, CD31, and CD309, acquired expression of MSC marker CD90 and more matured HSC/HPC or EPC marker CD34 until P6 (at least about 50 days), and maintained relative high proliferation rate of population doubling time. Previous studies on cultured human CD133$^+$ cells demonstrated a relatively faster rate of loss of CD133[38,44,60], and expansion of cultured human CD133$^+$ cells lead to CD90$^+$CD34$^-$ MSCs[38,60]. The observed difference might be due to the fact

that we expanded $CD133^+$ cells under conditions more specific for HSC/HPCs instead of EPCs or MSCs. The culture system in our study was based on previous studies with slightly modifications[39,44–46] and might provide a new approach to expand $CD133^+$ cells in vitro.

We also observed multipotency of $CD133^+$ cells towards neurogenic cell lineages and expression of significant robust neurotrophic factors compared with $CD133^-$ cells and BMNCs on the transcriptional level, which is consistent with previous studies of human $CD133^+$ stem cells[39,60,64]. Although the ability of HSC/HPCs to fully differentiate into endo- or ectodermal lineages is controversial[11,21], emerging evidence supports that $CD133^+$ cells have the potential to generate multiple functional cell lineages that have contributed to cell therapy in various degenerative diseases, including diabetes[34,35,41,65]. These data suggest that CD133 selection is useful for isolating the adult stem cells from bone marrow with neuroregenerative potential to home to site of injury and protect damaged tissue and cells.

Transplantation of $CD133^+$ Cells Prevents Visual Function Impairment and IR Degeneration in STZ-Induced Diabetic Mice

Emerging evidence demonstrated that identifying early neurodegeneration could be a sensitive biomarker for timely management of DR[10]. In our study, we found attenuated dark-adapted ERGs and OPs from D28 post-STZ with worsened duration of hyperglycemia for 84 days, which is consistent with the results from previous studies[14,61,62]. Thus we determined the cell-based therapeutic efficacy on visual functions at the early stage of DR on D28 and D56 post-transplantation.

We used ERG and optomotor responses to assess the therapeutic effects of $CD133^+$ cell transplantation on the visual function. Compared with PBS treatment, transplantation of $CD133^+$ cells significantly improved the b-wave but not the a-wave on both Post-D28 and Post-D56, whereas OPs on Post-D28 but not on Post-D56. Previous works reported different success only on ERGs in DR rodents treated with different cell types[21,26,27,31,32,66]. Our study also found that the visual acuity tested by optomotor responses showed significantly synchronous improvement in $CD133^+$ cell-treated group, which was consistent with improved ERG responses. The impaired retinal electrical responses were reported to relate to defected visual acuity in diabetic patients and animals[15,16]. Hence, this finding suggests a relationship of visual performance with electrophysiology of retinal functions, which is consistent with other study[16]. Moreover, according to previous studies, little or no significant improvement in ERG responses was detected with MSCs transplanted in diabetic rodents 84 days post-STZ[26,27,32]. This difference might be due to the different time point for intervention. As the time window is quite important for grafted stem cell to reverse or limit the structural damage in the retina[21], we introduced cells early on D28 post-STZ, when minimal retinopathy had occurred. A recent study revealed that umbilical cord MSC-induced neural stem cells displayed enhanced efficacy over MSCs on ERG responses when introduced on the 4th week post-STZ[31]. These results further indicate that cell-based intervention at an early stage can induce the timely rescue of visual dysfunction in DR mice.

To note, as MSCs are a heterogeneous population and usually form a clump of cells in the VC when intravitreally injected, transplantation of them could lead to the tractional retinal detachment[67]. In addition, the retinal gliosis, vascular obstruction and fibrovascular proliferation are recognized as the complications of MSC-based cell therapy in the retinal dysfunction[21]. However, these adverse effects were not observed in present $CD133^+$ cells transplantation in DR mice model.

Functional impairment synchronously occurred with underlying IR degeneration in DR[16,62,68,69]. In line with this, considering the ERG, optomotor responses and retina histological thickness data, we found that eyes with robust b-wave and OPs and better acuity had a thicker IR, particularly the thickness of IR, IPL, INL, OPL, together with a greater number of cells in the GCL. In addition, we observed that the surviving, transplanted $CD133^+$ cells gradually migrated from the VC to the IR over time. Along with the functional results, we suggest that transplanted $CD133^+$ cells may prevent visual loss by surviving and migrating to protect the IR in STZ mice. This result was consistent with a previous study demonstrating that treatment involving the prevention of GC-IPL degeneration by angiopoietin-1 is related to the improved ERG and visual acuity in diabetic mice[70]. Notably, we found significance of the a-wave amplitude but not on the ONL; the explanation might be that photoreceptors dysfunction instead of cell death has been detected and resulted in the decreased a-wave in diabetes[71].

Emerging evidence demonstrated that impaired scotopic b-wave and OPs reflect early changes in the rod pathway in the IR of diabetic rodents[62,68,69], including RGCs and RBCs[14–16,27]. Further investigations of IR neurons including RGCs and RBCs showed that, considering the results above, retinas after transplantation of $CD133^+$ cells with thicker IRs displayed a greater number and longer axons and dendrites of PKCα-positive cells and a greater expression of Tuj1 and PKCα, of which the staining of these markers extended from GCL to OPL in the retina. This finding has not been reported on previous studies with stem cell or other treatments for DR[26–28,31,70]. Thus considering all the results above, we suggested that, $CD133^+$ cell transplantation prevents the RGC and RBC degeneration in the IR, which results in thicker IR and improved ERG and optomotor responses in STZ mice with early stage DR. Notably, we examined only neuronal functions and structural changes based on reports that no obvious vascular changes or gliosis occur within 84 days post-STZ[14,61]. The vascular changes cannot be detected until 6 months and no neovascularization can be detected

due to the limited lifespan of mice[61]. Despite this limitation, this study suggests that CD133$^+$ cell exert therapeutic effects on visual functions in STZ-induced diabetic mice.

Since the number of transplanted cells in our study was limited and there were cell loss over time, the visual function especially OPs could not be preserved for a longer time as the development of DR proceeded. Further investigations should focus on repeated application of cells or optimal methods to increase the cell survival in vivo.

The neuroregenerative Potential of CD133$^+$ cells in STZ-Induced Diabetic Mice: Neural Differentiation and Neurotrophy

Although we confirmed the therapeutic effect of CD133$^+$ cells on retinal degeneration in DR mice at the early stage, the underlying mechanism remains unclear. The bone marrow has been reported to contain adult stem cells with the ability to regenerate damaged cells and tissues through cell replacement, trophic support and immunomodulation[21].

Mounting evidence has documented that CD133$^+$ EPCs can differentiate into endothelial cells for revascularization both in vitro and in vivo[39]. In the present study, we demonstrated the neural differentiation ability of CD133$^+$ cells in vitro and found that these cells migrated to the GCL and expressed the neural lineage marker Tuj1 after grafted into the STZ retinas. This finding differs from previous works on cell-based therapy for DR that demonstrated that cells such as MSCs have little or no efficacy to integrate or differentiate into the diabetic retina[26,27,31]. Recently, the notion that MSCs are able to trans-differentiate into neurons has been widely debated and negated[21]. Nevertheless, Harris et al. reported in vivo differentiation of mouse bone marrow-derived CD133$^+$ cells towards retinal pigment epithelial cells[63]. Growing evidence demonstrates that stem cells regenerate tissue or cells through cell fusion instead of differentiation[72]. In vivo reprogramming of terminally differentiated retinal neurons can occur after fusion with HSC/HPCs for tissue regeneration[73]. Despite the unclear mechanism of EGFP$^+$ cells co-expressed with retina neuron markers, in our study, we found even more cells in the GCL in the STZ+CD133$^+$ group than in the vehicle group. The possible explanation for this is the prevention of cell loss, proliferation of cells in the GCL, or recruitment of other cell types. Considering the results of increased cells, increased expression of Tuj1 and migration of CD133$^+$ cells in the GCL in our study, we suggest that transplanted CD133$^+$ cells may contribute to the increased expression of Tuj1 and directly or indirectly protect RGCs against death in STZ mice. However, it should be noted that our study only examined staining of specific markers, further studies are required to assess the functional integration of these cells, such as functional synapse formation. Moreover, since only approximately 50% of the neurons in the GCL of the mouse retina are RGCs[53], an exploration into other neuroretinal cell types such as amacrine cell as targets for CD133$^+$ cells treatment is merited.

A recent study demonstrated that direct cell replacement with a single cell type for reconstruction might have a limited therapeutic effect because the damaged retina should be regarded as a whole[21]. A previous study of human CD133$^+$ cells displayed the ability to induce regeneration of surrounding cells by paracrine molecules through correct location to injured sites[41]. In our study, given that the location of transplanted cells was mainly the GCL, the restoration of visual function due to engrafted cell differentiation might not be sufficient.

We found that CD133$^+$ cells could express robust neurotrophic factors genes at the transcriptional level (including NGF, BDNF, GDNF and CNTF, particularly BDNF) in vitro compared with CD133$^-$ cells. These neurotrophic factors were decreased and thus compromised neuroprotection in diabetes[8]. To enhance the expression and function of these neuroprotective factors synthesized by the retina could be a therapeutic target in DR[6,8]. In our study, we found that transplanted CD133$^+$ cells migrated to the GCL, expressed BDNF, and increased BDNF level in the cell-treated retinas compared with vehicle, STZ-untreated or PBS group. Previous studies have demonstrated a protective role of BDNF in the retina including RGCs and RBCs in retina degeneration[57] and DR[8,31]. BDNF could reach the INL and ONL, increase RGC survival in diabetic animals[31], and shape the dendrites of RBCs in a retina degeneration animal model[57]. Hence, we suggested that the preservation of visual function and IR degeneration in STZ-induced diabetic retina transplanted with CD133$^+$ cells might be involved in a BDNF-dependent mechanism to protect retinal neurons. Further studies to block or overexpress BDNF will help to investigate the precise mechanism, which might provide significant information regarding specific trophic factors that are indicated in the pathogenesis and prevention of DR.

In summary, this study reveals the neuronal regenerating potential of transplanted CD133$^+$ stem cells in DR at the early stages, including visual functional preservations with underlying structural inner retina amelioration in STZ-induced diabetic mice with DR. Further studies should extend the experimental time to evaluate the therapeutic efficacy of these cells at the late stage of DR on microvascular changes through the use of appropriate animal models and elucidate the specific underlying mechanism of the protective effect of CD133$^+$ stem cells on the retina with the aim of extending clinical applications.

Acknowledgments

The authors thank Akihiro Shimosaka (Asian Cellular Therapy Organization, Research Foundation for Community Medicine) for insightful and constructive discussions.

Ethical Approval

The study was approved by the Institutional Animal Care and Use Committee of Third Military Medical University, Chongqing, China.

Statement of Human and Animal Rights

All the related experiment procedures meet the requirements of Laboratory Animal Welfare and Ethics Committee of the Third Military Medical University.

Statement of Informed Consent

Statement of Informed Consent is not applicable.

Declaration of Conflicting Interests

The authors declared no potential conflicts of interest with respect to the research, authorship, and/or publication of this article.

Funding

The authors disclosed receipt of the following financial support for the research and/or authorship of this article: This work was supported by the National Key Basic Research Program of China (2013CB967002), the National Natural Science Foundation of China (81570890) and the Foundation of Southwest Hospital (SWH2016LHYS-03, SWH2016ZDCX1001, SWH2017ZDCX2007).

ORCID iD

Haiwei Xu http://orcid.org/0000-0002-8840-7918

Supplemental Material

Supplementary material for this article is available online.

References

1. Yau JW, Rogers SL, Kawasaki R, et al. Global prevalence and major risk factors of diabetic retinopathy. Diabetes Care. 2012; 35(3):556–564.
2. Cheung N, Mitchell P, Wong TY. Diabetic retinopathy. Lancet. 2010;376(9735):124–136.
3. Leasher JL, Bourne RR, Flaxman SR, Jonas JB, Keeffe J, Naidoo K, Pesudovs K, Price H, White RA, Wong TY, Resnikoff S, Taylor HR; Vision Loss Expert Group of the Global Burden of Disease S. Global estimates on the number of people blind or visually impaired by diabetic retinopathy: a meta–analysis from 1990 to 2010. Diabetes Care. 2016;39(9): 1643–1649.
4. Whiting DR, Guariguata L, Weil C, Shaw J. Idf diabetes atlas: global estimates of the prevalence of diabetes for 2011 and 2030. Diabetes Res Clin Pract. 2011;94(3):311–321.
5. Park YG, Roh YJ. New diagnostic and therapeutic approaches for preventing the progression of diabetic retinopathy. J Diabetes Res. 2016;2016:1753584.
6. Ezquer F, Ezquer M, Arango–Rodriguez M, Conget P. Could donor multipotent mesenchymal stromal cells prevent or delay the onset of diabetic retinopathy? Acta Ophthalmol. 2014; 92(2):e86–e95.
7. Jackson GR, Barber AJ. Visual dysfunction associated with diabetic retinopathy. Curr Diab Rep. 2010;10(5):380–384.
8. Simo R, Hernandez C; European Consortium for the Early Treatment of Diabetic R. Neurodegeneration in the diabetic eye: New insights and therapeutic perspectives. Trends Endocrinol Metab. 2014;25(1):23–33.
9. Barber AJ, Baccouche B. Neurodegeneration in diabetic retinopathy: potential for novel therapies. Vision Res. 2017;139: 82–92.
10. Verbraak FD. Neuroretinal degeneration in relation to vasculopathy in diabetes. Diabetes. 2014;63(11):3590–3592.
11. Kramerov AA, Ljubimov AV. Stem cell therapies in the treatment of diabetic retinopathy and keratopathy. Exp Biol Med (Maywood). 2016;241(6):559–568.
12. Megaw R, Dhillon B. Stem cell therapies in the management of diabetic retinopathy. Curr Diab Rep. 2014;14(7):498.
13. van Dijk HW, Kok PH, Garvin M, Sonka M, Devries JH, Michels RP, van Velthoven ME, Schlingemann RO, Verbraak FD, Abramoff MD. Selective loss of inner retinal layer thickness in type 1 diabetic patients with minimal diabetic retinopathy. Invest Ophthalmol Vis Sci. 2009;50(7):3404–3409.
14. Piano I, Novelli E, Della Santina L, Strettoi E, Cervetto L, Gargini C. Involvement of autophagic pathway in the progression of retinal degeneration in a mouse model of diabetes. Front Cell Neurosci. 2016;10:42.
15. Wang Y, Zhou Y, Xiao L, Zheng S, Yan N, Chen D. E2f1 mediates high glucose-induced neuronal death in cultured mouse retinal explants. Cell Cycle. 2017;16(19):1824–1834.
16. Moore-Dotson JM, Beckman JJ, Mazade RE, Hoon M, Bernstein AS, Romero-Aleshire MJ, Brooks HL, Eggers ED. Early retinal neuronal dysfunction in diabetic mice: Reduced light-evoked inhibition increases rod pathway signaling. Invest Ophthalmol Vis Sci. 2016;57(3):1418–1430.
17. Simo R, Hernandez C. Novel approaches for treating diabetic retinopathy based on recent pathogenic evidence. Prog Retin Eye Res. 2015;48:160–180.
18. Park H-YL, Kim JH, Park CK. Neuronal cell death in the inner retina and the influence of vascular endothelial growth factor inhibition in a diabetic rat model. Am J Pathol. 2014;184(6): 1752–1762.
19. Forbes JM, Cooper ME. Mechanisms of diabetic complications. Physiol Rev. 2013;93(1):137–188.
20. Liu Y, Chen SJ, Li SY, Qu LH, Meng XH, Wang Y, Xu HW, Liang ZQ, Yin ZQ. Long-term safety of human retinal progenitor cell transplantation in retinitis pigmentosa patients. Stem Cell Res Ther. 2017;8(1):209.
21. Park SS, Moisseiev E, Bauer G, Anderson JD, Grant MB, Zam A, Zawadzki RJ, Werner JS, Nolta JA. Advances in bone marrow stem cell therapy for retinal dysfunction. Prog Retin Eye Res. 2017;56:148–165.
22. Yellowlees Douglas J, Bhatwadekar AD, Li Calzi S, Shaw LC, Carnegie D, Caballero S, Li Q, Stitt AW, Raizada MK, Grant MB. Bone marrow–cns connections: Implications in the pathogenesis of diabetic retinopathy. Prog Retin Eye Res. 2012; 31(5):481–494.
23. Bhatwadekar AD, Glenn JV, Li G, Curtis TM, Gardiner TA, Stitt AW. Advanced glycation of fibronectin impairs vascular repair by endothelial progenitor cells: Implications for vasodegeneration in diabetic retinopathy. Invest Ophthalmol Visual Sci. 2008;49(3):1232–1241.
24. Ferraro F, Lymperi S, Mendez-Ferrer S, Saez B, Spencer JA, Yeap BY, Masselli E, Graiani G, Prezioso L, Rizzini EL,

Mangoni M, Rizzoli V, Sykes SM, Lin CP, Frenette PS, Quaini F, Scadden DT. Diabetes impairs hematopoietic stem cell mobilization by altering niche function. Sci Transl Med. 2011;3(104):104ra101.
25. Shaw LC, Neu MB, Grant MB. Cell-based therapies for diabetic retinopathy. Curr Diab Rep. 2011;11(4):265–274.
26. Cerman E, Akkoc T, Eraslan M, Sahin O, Ozkara S, Vardar Aker F, Subasi C, Karaoz E, Akkoc T. Retinal electrophysiological effects of intravitreal bone marrow-derived mesenchymal stem cells in streptozotocin induced diabetic rats. PLoS One. 2016;11(6):e0156495.
27. Ezquer M, Urzua CA, Montecino S, Leal K, Conget P, Ezquer F. Intravitreal administration of multipotent mesenchymal stromal cells triggers a cytoprotective microenvironment in the retina of diabetic mice. Stem Cell Res Ther. 2016;7:42.
28. Yang Z, Li K, Yan X, Dong F, Zhao C. Amelioration of diabetic retinopathy by engrafted human adipose–derived mesenchymal stem cells in streptozotocin diabetic rats. Graefes Arch Clin Exp Ophthalmol. 2010; 248(10):1415–1422.
29. Kim JM, Hong KS, Song WK, Bae D, Hwang IK, Kim JS, Chung HM. Perivascular progenitor cells derived from human embryonic stem cells exhibit functional characteristics of pericytes and improve the retinal vasculature in a rodent model of diabetic retinopathy. Stem Cells Transl Med. 2016;5(9): 1268–1276.
30. Yu Z, Zhang T, Gong C, Sheng Y, Lu B, Zhou L, Ji L, Wang Z. Erianin inhibits high glucose-induced retinal angiogenesis via blocking erk1/2-regulated hif–1alpha–vegf/vegfr2 signaling pathway. Sci Rep. 2016;6:34306.
31. Zhang W, Wang Y, Kong J, Dong M, Duan H, Chen S. Therapeutic efficacy of neural stem cells originating from umbilical cord–derived mesenchymal stem cells in diabetic retinopathy. Sci Rep. 2017;7(1):408.
32. Rajashekhar G, Ramadan A, Abburi C, Callaghan B, Traktuev DO, Evans-Molina C, Maturi R, Harris A, Kern TS, March KL. Regenerative therapeutic potential of adipose stromal cells in early stage diabetic retinopathy. PLoS One. 2014;9(1):e84671.
33. Wang JD, An Y, Zhang S, Wan H, Jonas JB, Xu L, Zhang W. Human bone marrow mesenchymal stem cells for retinal vascular injury. Acta Ophthalmologica. 2017;95(6):e453–e461.
34. Li Z. Cd133: a stem cell biomarker and beyond. Exp Hematol Oncol. 2013;2(1):17.
35. Meregalli M, Farini A, Belicchi M, Torrente Y. Cd133(+) cells for the treatment of degenerative diseases: Update and perspectives. Adv Exp Med Biol. 2013;777:229–243.
36. Friedrich EB, Walenta K, Scharlau J, Nickenig G, Werner N. Cd34–/cd133+/vegfr–2+ endothelial progenitor cell subpopulation with potent vasoregenerative capacities. Circ Res. 2006; 98(3):e20–e25.
37. Germano D, Blyszczuk P, Valaperti A, Kania G, Dirnhofer S, Landmesser U, Luscher TF, Hunziker L, Zulewski H, Eriksson U. Prominin–1/cd133+ lung epithelial progenitors protect from bleomycin–induced pulmonary fibrosis. Am J Respir Crit Care Med. 2009;179(10):939–949.
38. Bakondi B, Shimada IS, Perry A, Munoz JR, Ylostalo J, Howard AB, Gregory CA, Spees JL. Cd133 identifies a human bone marrow stem/progenitor cell subpopulation with a repertoire of secreted factors that protect against stroke. Mol Ther. 2009;17(11):1938–1947.
39. Kamei N, Kwon SM, Alev C, Nakanishi K, Yamada K, Masuda H, Ishikawa M, Kawamoto A, Ochi M, Asahara T. Ex-vivo expanded human blood-derived cd133+ cells promote repair of injured spinal cord. J Neurol Sci. 2013;328(1–2): 41–50.
40. Steinhoff G, Nesteruk J, Wolfien M, et al. Cardiac function improvement and bone marrow response –: Outcome analysis of the randomized perfect phase iii clinical trial of intramyocardial cd133+ application after myocardial infarction. EBioMedicine. 2017; 22:208–224.
41. Barcelos LS, Duplaa C, Krankel N, Graiani G, Invernici G, Katare R, Siragusa M, Meloni M, Campesi I, Monica M, Simm A, Campagnolo P, Mangialardi G, Stevanato L, Alessandri G, Emanueli C, Madeddu P. Human cd133+ progenitor cells promote the healing of diabetic ischemic ulcers by paracrine stimulation of angiogenesis and activation of wnt signaling. Circ Res. 2009;104(9):1095–1102.
42. Sasaki H, Ishikawa M, Tanaka N, Nakanishi K, Kamei N, Asahara T, Ochi M. Administration of human peripheral blood-derived cd133+ cells accelerates functional recovery in a rat spinal cord injury model. Spine (Phila Pa 1976). 2009;34(3):249–254.
43. Mahajan MM, Cheng B, Beyer AI, Mulvaney US, Wilkinson MB, Fomin ME, Muench MO. A quantitative assessment of the content of hematopoietic stem cells in mouse and human endosteal-bone marrow: a simple and rapid method for the isolation of mouse central bone marrow. BMC Hematol. 2015;15:9.
44. Kuci S, Wessels JT, Buhring HJ, Schilbach K, Schumm M, Seitz G, Loffler J, Bader P, Schlegel PG, Niethammer D, Handgretinger R. Identification of a novel class of human adherent cd34- stem cells that give rise to scid-repopulating cells. Blood. 2003;101(3):869–876.
45. Carter DA, Dick AD, Mayer EJ. Cd133+ adult human retinal cells remain undifferentiated in leukaemia inhibitory factor (lif). BMC Ophthalmol. 2009;9:1.
46. Heo JS, Kim HO, Song SY, Lew DH, Choi Y, Kim S. Poly-l-lysine prevents senescence and augments growth in culturing mesenchymal stem cells ex vivo. BioMed Res Intern. 2016; 2016:8196078.
47. Chen X, Chen Z, Li Z, Zhao C, Zeng Y, Zou T, Fu C, Liu X, Xu H, Yin ZQ. Grafted c-kit+/ssea1- eye-wall progenitor cells delay retinal degeneration in mice by regulating neural plasticity and forming new graft-to-host synapses. Stem Cell Res Ther. 2016;7(1):191.
48. Corti S, Nizzardo M, Nardini M, Donadoni C, Locatelli F, Papadimitriou D, Salani S, Del Bo R, Ghezzi S, Strazzer S, Bresolin N, Comi GP. Isolation and characterization of murine neural stem/progenitor cells based on prominin-1 expression. Exp Neurol. 2007;205(2):547–562.
49. Chen X, Li Q, Xu H, Yin ZQ. Sodium iodate influences the apoptosis, proliferation and differentiation potential of radial

glial cells in vitro. Cell Physiol Biochem. 2014;34(4): 1109–1124.
50. Li Z, Zeng Y, Chen X, Li Q, Wu W, Xue L, Xu H, Yin ZQ. Neural stem cells transplanted to the subretinal space of rd1 mice delay retinal degeneration by suppressing microglia activation. Cytotherapy. 2016;18(6):771–784.
51. Gao L, Chen X, Tang Y, Zhao J, Li Q, Fan X, Xu H, Yin ZQ. Neuroprotective effect of memantine on the retinal ganglion cells of appswe/ps1deltae9 mice and its immunomodulatory mechanisms. Exp Eye Res. 2015;135:47–58.
52. Xie J, Huo S, Li Y, Dai J, Xu H, Yin ZQ. Olfactory ensheathing cells inhibit gliosis in retinal degeneration by downregulation of the muller cell notch signaling pathway. Cell Trans. 2017; 26(6):967–982.
53. Akopian A, Kumar S, Ramakrishnan H, Roy K, Viswanathan S, Bloomfield SA. Targeting neuronal gap junctions in mouse retina offers neuroprotection in glaucoma. J Clin Invest. 2017; 127(7):2647–2661.
54. Pearson RA, Barber AC, Rizzi M, Hippert C, Xue T, West EL, Duran Y, Smith AJ, Chuang JZ, Azam SA, Luhmann UF, Benucci A, Sung CH, Bainbridge JW, Carandini M, Yau KW, Sowden JC, Ali RR. Restoration of vision after transplantation of photoreceptors. Nature. 2012;485(7396):99–103.
55. Seiler MJ, Lin RE, McLelland BT, Mathur A, Lin B, Sigman J, De Guzman AT, Kitzes LM, Aramant RB, Thomas BB. Vision recovery and connectivity by fetal retinal sheet transplantation in an immunodeficient retinal degenerate rat model. Invest Ophthalmol Vis Sci. 2017;58(1):614–630.
56. Hertz J, Qu B, Hu Y, Patel RD, Valenzuela DA, Goldberg JL. Survival and integration of developing and progenitor-derived retinal ganglion cells following transplantation. Cell Transplant. 2014;23(7):855–872.
57. Fu Y, Hou B, Weng C, Liu W, Dai J, Zhao C, Yin ZQ. Functional ectopic neuritogenesis by retinal rod bipolar cells is regulated by mir-125b-5p during retinal remodeling in RCS rats. Sci Rep. 2017;7(1):1011.
58. Akopian A, Atlasz T, Pan F, Wong S, Zhang Y, Volgyi B, Paul DL, Bloomfield SA. Gap junction-mediated death of retinal neurons is connexin and insult specific: a potential target for neuroprotection. J Neurosci. 2014;34(32): 10582–10591.
59. Coskun V, Wu H, Blanchi B, Tsao S, Kim K, Zhao J, Biancotti JC, Hutnick L, Krueger RC Jr., Fan G, de Vellis J, Sun YE. Cd133+ neural stem cells in the ependyma of mammalian postnatal forebrain. Proc Natl Acad Sci USA. 2008;105(3): 1026–1031.
60. Pozzobon M, Piccoli M, Ditadi A, Bollini S, Destro R, Andre-Schmutz I, Masiero L, Lenzini E, Zanesco L, Petrelli L, Cavazzana-Calvo M, Gazzola MV, De Coppi P. Mesenchymal stromal cells can be derived from bone marrow cd133+ cells: Implications for therapy. Stem Cells Dev. 2009;18(3): 497–510.
61. Ramos D, Carretero A, Navarro M, Mendes-Jorge L, Rodriguez-Baeza A, Nacher V, Ruberte J. Mouse models of diabetic retinopathy. Drug Discov Today: Disease Mod. 2013;10(4): e195–e206.
62. Aung MH, Kim MK, Olson DE, Thule PM, Pardue MT. Early visual deficits in streptozotocin-induced diabetic long evans rats. Invest Opthalmol Visual Sci. 2013;54(2):1370.
63. Harris JR, Fisher R, Jorgensen M, Kaushal S, Scott EW. Cd133 progenitor cells from the bone marrow contribute to retinal pigment epithelium repair. Stem Cells. 2009;27(2):457–466.
64. Alessandri G, Pagano S, Bez A, Benetti A, Pozzi S, Iannolo G, Baronio M, Invernici G, Caruso A, Muneretto C, Bisleri G, Parati E. Isolation and culture of human muscle-derived stem cells able to differentiate into myogenic and neurogenic cell lineages. The Lancet. 2004;364(9448):1872–1883.
65. Meregalli M, Farini A, Belicchi M, Torrente Y. Cd133(+) cells isolated from various sources and their role in future clinical perspectives. Expert Opin Biol Ther. 2010;10(11):1521–1528.
66. Bhatwadekar AD, Duan Y, Korah M, Thinschmidt JS, Hu P, Leley SP, Caballero S, Shaw L, Busik J, Grant MB. Hematopoietic stem/progenitor involvement in retinal microvascular repair during diabetes: Implications for bone marrow rejuvenation. Vision Res. 2017;139:211–220.
67. Tzameret A, Sher I, Belkin M, Treves AJ, Meir A, Nagler A, Levkovitch-Verbin H, Barshack I, Rosner M, Rotenstreich Y. Transplantation of human bone marrow mesenchymal stem cells as a thin subretinal layer ameliorates retinal degeneration in a rat model of retinal dystrophy. Exp Eye Res. 2014;118: 135–144.
68. Pardue MT, Barnes CS, Kim MK, Aung MH, Amarnath R, Olson DE, Thule PM. Rodent hyperglycemia-induced inner retinal deficits are mirrored in human diabetes. Transl Vis Sci Technol. 2014;3(3):6.
69. Castilho A, Ambrosio AF, Hartveit E, Veruki ML. Disruption of a neural microcircuit in the rod pathway of the mammalian retina by diabetes mellitus. J Neurosci. 2015;35(13): 5422–5433.
70. Cahoon JM, Rai RR, Carroll LS, et al. Intravitreal aav2.Compang1 prevents neurovascular degeneration in a murine model of diabetic retinopathy. Diabetes. 2015;64(12):4247–4259.
71. Kern TS, Berkowitz BA. Photoreceptors in diabetic retinopathy. J Diabetes Investig. 2015;6(4):371–380.
72. Lluis F, Cosma MP. Cell-fusion-mediated somatic-cell reprogramming: A mechanism for tissue regeneration. J Cell Physiol. 2010;223(1):6–13.
73. Sanges D, Romo N, Simonte G, Di Vicino U, Tahoces AD, Fernandez E, Cosma MP. Wnt/beta-catenin signaling triggers neuron reprogramming and regeneration in the mouse retina. Cell Rep. 2013;4(2):271–286.